



Discovery of secondary sulphonamides as IDO1 inhibitors with potent antitumour effects *in vivo*

Shushan Ge^{a*} , Haiqing Zhong^{b*}, Xuewei Ma^{a*}, Yingbo Zheng^a, Yi Zou^a, Fang Wang^a, Yan Wang^b, Yue Hu^b, Yuezhen Li^c, Wen Liu^b, Wenjie Guo^b , Qiang Xu^b and Yisheng Lai^a 

^aState Key Laboratory of Natural Medicines, Jiangsu Key Laboratory of Drug Discovery for Metabolic Diseases, Center of Drug Discovery, China Pharmaceutical University, Nanjing, PR China; ^bState Key Laboratory of Pharmaceutical Biotechnology, School of Life Sciences, Nanjing University, Nanjing, PR China; ^cDepartment of Organic Chemistry, School of Science, China Pharmaceutical University, Nanjing, PR China

ABSTRACT

Indoleamine 2,3-dioxygenase 1 (IDO1) as a key rate-limiting enzyme in the kynurenine pathway of tryptophan metabolism plays an important role in tumour immune escape. Herein, a variety of secondary sulphonamides were synthesised and evaluated in the HeLa cell-based IDO1/kynurenine assay, leading to the identification of new IDO1 inhibitors. Among them, compounds **5d**, **5l** and **8g** exhibited the strongest inhibitory effect with significantly improved activity over the hit compound BS-1. The *in vitro* results showed that these compounds could restore the T cell proliferation and inhibit the differentiation of naïve CD4⁺ T cell into highly immunosuppressive FoxP3⁺ regulatory T (Treg) cell without affecting the viability of HeLa cells and the expression of IDO1 protein. Importantly, the pharmacodynamic assay showed that compound **5d** possessed potent antitumour effect in both CT26 and B16F1 tumours bearing immunocompetent mice but not in immunodeficient mice. Functionally, subsequent experiments demonstrated that compound **5d** could effectively inhibit tumour cell proliferation, induce apoptosis, up-regulate the expression of IFN- γ and granzyme B, and suppress FoxP3⁺ Treg cell differentiation, thereby activate the immune system. Thus, compound **5d** could be a potential and efficacious agent for further evaluation.

ARTICLE HISTORY

Received 27 February 2020
Revised 29 April 2020
Accepted 30 April 2020

KEYWORDS

Indoleamine 2,3-dioxygenase 1; kynurenine pathway; immune escape; immune checkpoint; secondary sulphonamides

1. Introduction

With the increasing recognition of the interaction between the immune system and tumour cells, immunotherapy has gained tremendous attention in the field of cancer research^{1,2}. The recent clinical successes of immune checkpoint inhibitors and chimeric antigen receptor T cell (CAR-T) therapy have dramatically changed the landscape of the cancer treatment^{3–6}. To date, the US Food and Drug Administration (FDA) has approved six immune checkpoint inhibitors blocking cytotoxic T lymphocyte-associated antigen 4 (CTLA-4), programmed cell death protein 1 (PD-1) or programmed cell death ligand 1 (PD-L1), and the second CAR-T cell therapy for the treatment of solid and hematological malignancies. However, their limited response rate and immune-related adverse effects call for a need to develop other immunotherapy options to solve those problems^{5–7}.

Indoleamine 2,3-dioxygenase 1 (IDO1) is a haem-containing enzyme that catalyses the initial and rate-limiting step in the catabolism of the essential amino acid tryptophan along the kynurenine pathway⁸. IDO1 plays an important role in the regulation of local inflammation and immune tolerance⁹. In cancer, aberrant activation of IDO1 results in suppression of antitumour immunity. The depletion of tryptophan and the accumulation of kynurenine and its downstream metabolites in the tumour

microenvironment have been demonstrated to induce effector T cell anergy and enhance regulatory T (Treg) cell function, which eventually lead to an immunosuppressive milieu that helps tumour cells evade detection and killing by the immune system¹⁰. Tryptophan depletion has been implicated in the activation of general control non-repressible 2 (GCN2) and suppression of the mechanistic target of rapamycin kinase (mTOR) pathways^{11,12}. Furthermore, kynurenine and other tryptophan metabolites can activate the aryl hydrocarbon receptor (AHR)¹³. Indeed, high expression of IDO1 in tumour cells has been shown to correlate with worse clinical prognosis in patients with a variety of cancers, including colorectal, ovarian, endometrial, and hepatocellular carcinomas^{14–18}. Moreover, preclinical studies have demonstrated that IDO inhibitors can effectively restore antitumour immunity and have the potential to synergize with chemotherapy, radiotherapy, and other immunotherapies, including anti-CTLA-4, anti-PD-1 and anti-PD-L1 antibodies^{19–22}. Hence, these findings have motivated interest in developing IDO1 inhibitors for cancer immunotherapy.

So far, a number of IDO1 inhibitors have been identified from high-throughput screening^{23,24}, structure-based design^{25–27}, and natural product screening^{28,29}. Several of them, including, navoximod, epacadostat, PF-06840003, linrodostat, LY-3381916 and KHK2455 (structure not disclosed), have entered clinical development as monotherapy and in combination with other immune

CONTACT Wenjie Guo  guowj@nju.edu; Qiang Xu  molpharm@163.com  State Key Laboratory of Pharmaceutical Biotechnology, School of Life Sciences, Nanjing University, Nanjing 210093, PR China; Yisheng Lai  yslai@cpu.edu.cn  State Key Laboratory of Natural Medicines, Jiangsu Key Laboratory of Drug Discovery for Metabolic Diseases, Center of Drug Discovery, China Pharmaceutical University, Nanjing, 210009, PR China

*These contributed equally to this article.

© 2020 The Author(s). Published by Informa UK Limited, trading as Taylor & Francis Group.

This is an Open Access article distributed under the terms of the Creative Commons Attribution License (<http://creativecommons.org/licenses/by/4.0/>), which permits unrestricted use, distribution, and reproduction in any medium, provided the original work is properly cited.

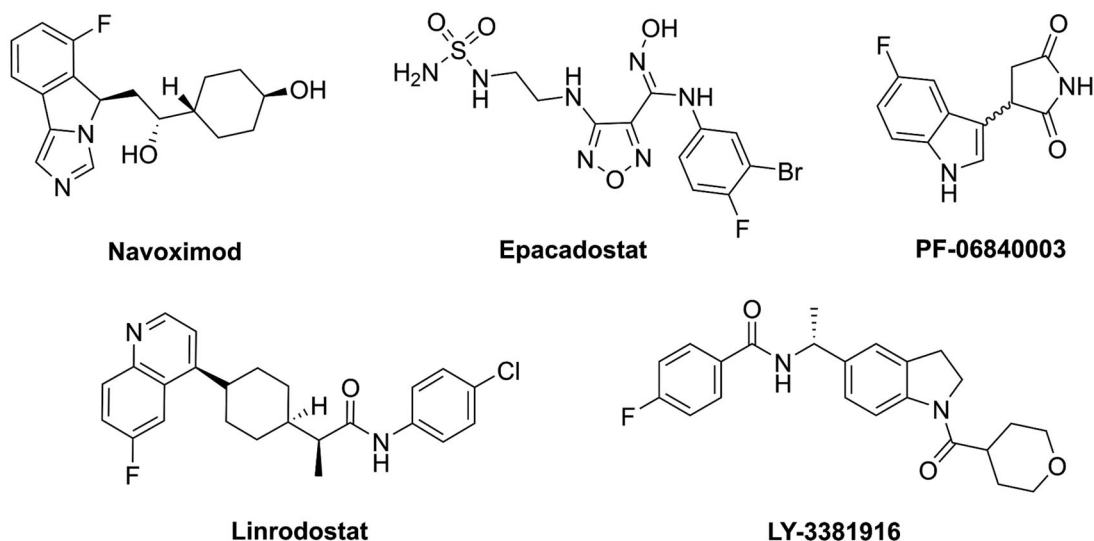


Figure 1. Structure of representative IDO1 clinical candidates.

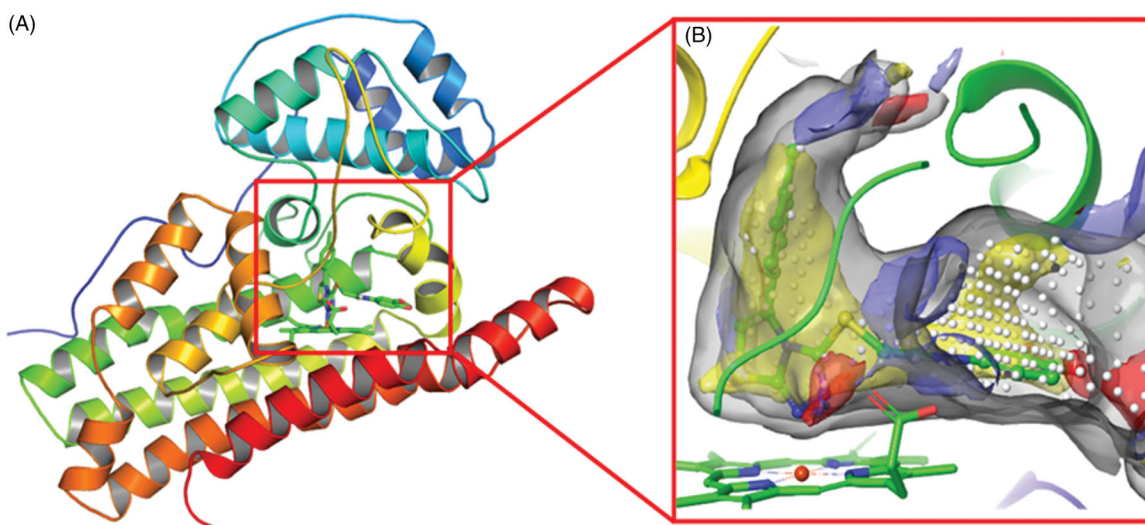


Figure 2. (A) The co-crystal of IDO1 (PDB ID: 4PK5). (B) Site maps generated using Sitemap: the ligand was Amg-1, white points represented the new identified active region, as well as yellow, blue and red solid maps represented hydrophobic regions, hydrogen bond donors and acceptors, respectively.

therapies or chemotherapy (Figure 1)³⁰. However, the FDA has not yet approved IDO inhibitors for the treatment of malignancies to date. We therefore need to continue to identify novel IDO1 inhibitors.

In recent years, we have been working on the development of novel IDO1 inhibitors^{31–34}. From our previous study on the interactions between IDO1 and imidazole derivatives, it has been found that metal chelation, hydrogen bonding, and hydrophobic interactions between haem and the ligand contribute a large proportion to the binding affinity of the inhibitor³¹. Furthermore, the human IDO1 crystal structures in complex with the ligand Amg-1 (PDB ID: 4PK5) revealed that IDO1 is characterised by a small and highly lipophilic active site including two pockets (A and B), implying that the hydrophobic interaction may account for a large part of protein-ligand nonbonding interactions (Figure 2). In addition, Muller's team demonstrated that as the charge on the coordinating atom decreased, the binding affinity to the haem iron increased, which would be possible to improve IDO1 inhibitory activity³⁵. These findings provide directions for improving the binding affinity of novel IDO1 inhibitors.

In this study, we screened our in-house compound library using the HeLa cell-based IDO1/kynurenine assay, and found that the

secondary sulphonamide compound BS-1 showed inhibitory activity against IDO1 with an IC_{50} value of 48.42 μ M. As well known, bezenesulfonamide is a common pharmacophore that is the basis of several groups of drugs, such as sulpha antibiotics, thiazide diuretics and nonsteroidal antiinflammatory drug (NSAID) celecoxib^{36,37}. Moreover, the sulphonyl is a heme-binding function that coordinates to the haem iron of IDO1³⁸. Therefore, the hit compound BS-1 was further modified, as well as a variety of secondary sulphonamides were synthesised and evaluated in the HeLa cell-based IDO1/kynurenine assay. The resulting compounds **5d**, **5l** and **8g** showed high inhibitory activity without affecting the cell viability and the IDO1 protein expression. Subsequent *in vitro* and *in vivo* experiments demonstrated that compound **5d** could exert potent antitumour effects by activating the mouse immune system.

2. Material and methods

2.1. Chemistry

Melting points were determined on a RDCSY-I capillary apparatus and were uncorrected. All materials used were commercially

available and used as supplied. HG/T2354-92 silica gel 60 F254 sheets were used for analytical thin-layer chromatography (TLC). Column chromatography was performed on silica gel (300–400 mesh). ^1H NMR spectra were recorded on a Bruker AV-300 spectrometer. Chemical shifts (δ) were given in parts per million (ppm) relative to the solvent peak. J values are in Hz. Chemical shifts are expressed in ppm downfield from internal standard TMS. Mass spectra (MS) were measured using a Thermo Scientific iCAP RQ ICP-MS. All the reagents and solvents were reagent grade and were used without further purification unless otherwise specified.

2.1.1. General preparation of compounds 3a-i

To a solution of substituted aniline (0.97 mmol) in DCM (15 ml) was added triethylamine (1.22 mmol)³⁹. A solution of 4-acrylamidobenzenesulfonyl chloride (0.81 mmol) in DCM (10 ml) was added dropwise to the mixture at 0 °C. The reaction was stirred at room temperature for 4 h. The solvent was evaporated under reduced pressure and the crude product was recrystallization to afford target compounds **3a-i**.

2.1.1.1. N-(4-(N-Phenylsulfamoyl)phenyl)acetamide (3a). White solid. Yield 90%. Mp 204–206 °C. ^1H NMR (300 MHz, DMSO- d_6) δ 10.17 (s, 1H), 10.04 (s, 1H), 7.54 (s, 4H), 7.08 (t, $J=7.8$ Hz, 2H), 6.94–6.84 (m, 3H), 1.91 (s, 3H). MS (EI) m/z 289.1 [M-H]⁻.

2.1.1.2. N-(4-(N-(p-Tolyl)sulfamoyl)phenyl)acetamide (3b). White solid. Yield 87%. Mp > 250 °C. ^1H NMR (300 MHz, DMSO- d_6) δ 10.45 (s, 1H), 9.89 (s, 1H), 7.69 (d, $J=8.1$ Hz, 2H), 7.57 (d, $J=8.4$ Hz, 2H), 7.08 (d, $J=7.8$ Hz, 2H), 6.73 (d, $J=7.8$ Hz, 2H), 2.19 (s, 3H), 1.92 (s, 3H). MS (EI) m/z 303.1 [M-H]⁻.

2.1.1.3. N-(4-(N-(4-Isopropylphenyl)sulfamoyl)phenyl)acetamide (3c). Light yellow solid, Yield 90%, Mp 186–188 °C. ^1H NMR (300 MHz, DMSO- d_6) δ 10.16 (s, 1H), 9.91 (s, 1H), 7.54 (s, 4H), 6.95 (d, $J=8.1$ Hz, 2H), 6.94 (d, $J=8.1$ Hz, 2H), 2.65–2.58 (m, 1H), 1.92 (d, $J=2.4$ Hz, 3H), 0.97 (dd, $J=2.1, 2.7$ Hz, 6H). MS (EI) m/z 331.1 [M-H]⁻.

2.1.1.4. N-(4-(N-(3-Isopropylphenyl)sulfamoyl)phenyl)acetamide (3d). White solid. Yield 90%. Mp 158–160 °C. ^1H NMR (300 MHz, DMSO- d_6) δ 10.17 (s, 1H), 9.95 (s, 1H), 7.55 (s, 4H), 6.98 (t, $J=7.7$ Hz, 1H), 6.79–6.72 (m, 3H), 2.63–2.58 (m, 1H), 1.92 (s, 3H), 0.95 (d, $J=6.9$ Hz, 6H). MS (EI) m/z 331.1 [M-H]⁻.

2.1.1.5. N-(4-(N-Benzylsulfamoyl)phenyl)acetamide (3e). White solid. Yield 90%. Mp 140–142 °C. ^1H NMR (300 MHz, DMSO- d_6) δ 10.20 (s, 1H), 7.89 (t, $J=6.3$ Hz, 1H), 7.64–7.57 (m, 4H), 7.18–7.07 (m, 5H), 3.81 (d, $J=6.3$ Hz, 2H), 1.96 (s, 3H). MS (EI) m/z 303.1 [M-H]⁻.

2.1.1.6. N-(4-(N-(4-Chlorobenzyl)sulfamoyl)phenyl)acetamide (3f). White solid. Yield 90%. Mp 172–174 °C. ^1H NMR (300 MHz, DMSO- d_6) δ 10.20 (s, 1H), 7.95 (t, $J=6.5$ Hz, 1H), 7.63–7.56 (m, 4H), 7.17 (dd, $J=8.1, 8.4$ Hz, 4H), 3.81 (d, $J=6.3$ Hz, 2H), 1.95 (s, 3H). MS (EI) m/z 337.1 [M-H]⁻.

2.1.1.7. N-(4-(N-(4-Trifluoromethyl)benzyl)sulfamoyl)phenyl) acetamide (3g). White solid. Yield 89%. Mp 186–188 °C. ^1H NMR (300 MHz, DMSO- d_6) δ 10.19 (s, 1H), 8.04 (t, $J=6.0$ Hz, 1H), 7.62–7.56 (m, 4H), 7.50 (d, $J=8.1$ Hz, 2H), 7.33 (d, $J=8.1$ Hz, 2H), 3.93 (d, $J=5.7$ Hz, 2H), 1.95 (s, 3H). MS (EI) m/z 371.1 [M-H]⁻.

2.1.1.8. N-(4-(N-(3-(Trifluoromethyl)benzyl)sulfamoyl)phenyl)acetamide (3h). White solid. Yield 88%. Mp 154–156 °C. ^1H NMR (300 MHz, DMSO- d_6) δ 10.19 (s, 1H), 8.05 (t, $J=6.3$ Hz, 1H), 7.61–7.54 (m, 4H), 7.46–7.35 (m, 4H), 3.95 (d, $J=6.3$ Hz, 2H), 1.95 (s, 3H). MS (EI) m/z 371.1 [M-H]⁻.

2.1.1.9. N-(4-(N-Phenethylsulfamoyl)phenyl)acetamide (3i). White solid. Yield 85%. Mp 130–132 °C. ^1H NMR (300 MHz, DMSO- d_6) δ 10.19 (s, 1H), 7.59 (q, $J=8.5$ Hz, 4H), 7.46 (t, $J=5.9$ Hz, 1H), 7.16–7.00 (m, 5H), 2.82–2.75 (m, 2H), 2.52 (t, $J=7.5$ Hz, 2H), 1.95 (s, 3H). MS (EI) m/z 317.2 [M-H]⁻.

2.1.2. General preparation of compounds 4a-f

To a solution of compounds **3** (0.68 mmol) in ethanol (15 ml) was added hydrochloric acid (1 ml)³⁹. Then the mixture was stirred at 70 °C for 12 h. After the reaction was completed, the solvent was evaporated under reduced pressure. Water was added and the pH was adjusted to 7–8 with saturated NaHCO₃ solution. The aqueous phase was extracted with EtOAc (3 × 30 ml). The combined organic layers were washed with water, brine, and dried. The solvent was removed *in vacuo* and the crude product was recrystallization to afford target compounds **4a-f**.

2.1.2.1. 4-Amino-N-phenylbenzenesulfonamide (4a). Light yellow solid. Yield 89%. Mp 188–190 °C. ^1H NMR (300 MHz, DMSO- d_6) δ 9.81 (s, 1H), 7.34 (d, $J=8.6$ Hz, 2H), 7.15 (t, $J=7.8$ Hz, 2H), 7.01 (d, $J=7.7$ Hz, 2H), 6.94 (d, $J=7.3$ Hz, 1H), 6.48 (d, $J=8.7$ Hz, 2H), 5.92 (s, 2H). MS (EI) m/z 247.1 [M-H]⁻.

2.1.2.2. 4-Amino-N-(p-tolyl)benzenesulfonamide (4b). White solid. Yield 89%. Mp 188–190 °C. ^1H NMR (300 MHz, DMSO- d_6) δ 9.55 (s, 1H), 7.21 (d, $J=8.5$ Hz, 2H), 6.83 (dd, $J=8.0, 8.3$ Hz, 4H), 6.37 (d, $J=8.6$ Hz, 2H), 5.82 (s, 2H), 2.03 (s, 3H). MS (EI) m/z 261.1 [M-H]⁻.

2.1.2.3. 4-Amino-N-benzylbenzenesulfonamide (4c). White solid. Yield 93%. Mp 116–118 °C. ^1H NMR (300 MHz, DMSO- d_6) δ 7.53 (t, $J=6.1$ Hz, 1H), 7.32 (d, $J=8.6$ Hz, 2H), 7.09–7.18 (m, 5H), 6.49 (d, $J=8.6$ Hz, 2H), 3.73 (d, $J=5.9$ Hz, 2H). MS (EI) m/z 261.1 [M-H]⁻.

2.1.2.4. 4-Amino-N-(4-chlorobenzyl)benzenesulfonamide (4d). White solid. Yield 95%. Mp 172–174 °C. ^1H NMR (300 MHz, DMSO- d_6) δ 7.66 (t, $J=6.2$ Hz, 1H), 7.21–7.40 (m, 6H), 6.56 (d, $J=8.4$ Hz, 2H), 5.91 (s, 2H), 3.83 (d, $J=6.2$ Hz, 2H). MS (EI) m/z 295.1 [M-H]⁻.

2.1.2.5. 4-Amino-N-(3-chlorobenzyl)benzenesulfonamide (4e). White solid. Yield 90%. Mp 119–121 °C. ^1H NMR (300 MHz, DMSO- d_6) δ 7.70 (s, 1H), 7.42 (d, $J=8.6$ Hz, 2H), 7.36–7.11 (m, 4H), 6.60 (d, $J=8.4$ Hz, 2H), 5.92 (s, 2H), 3.90 (d, $J=5.0$ Hz, 2H). MS (EI) m/z 295.1 [M-H]⁻.

2.1.2.6. 4-Amino-N-phenethylbenzenesulfonamide (4f). White solid. Yield 90%. Mp 138–140 °C. ^1H NMR (300 MHz, DMSO- d_6) δ 7.37 (d, $J=8.4$ Hz, 2H), 7.14–7.25 (m, 5H), 6.56 (d, $J=8.5$ Hz, 2H), 2.82 (m, 2H), 2.60 (t, $J=7.4$ Hz, 2H). MS (EI) m/z 275.1 [M-H]⁻.

2.1.3. General preparation of compounds 5a-m

To a solution of compounds **4** (0.55 mmol) in DCM (15 ml) was added TEA (1.1 mmol). Then acryloyl chloride (0.61 mmol) was added dropwise to the mixture at 0 °C for 0.5 h. The reaction was stirred at rt overnight. After the reaction was completed, the

water was added to quench the reaction. The mixture was extracted with DCM to afford the crude product. The crude residue was recrystallization to afford target compounds **5a-m**.

2.1.3.1. N-(4-(N-Benzylsulfamoyl)phenyl)acrylamide (5a). White solid. Yield 75%. Mp 116–118 °C. ¹H NMR (300 MHz, DMSO-*d*₆) δ 10.50 (s, 1H), 8.02 (t, *J* = 6.2 Hz, 1H), 7.81 (d, *J* = 8.7 Hz, 2H), 7.72 (d, *J* = 8.7 Hz, 2H), 7.27–7.16 (m, 5H), 6.48–6.39 (m, 1H), 6.28 (d, *J* = 15.6 Hz, 1H), 5.79 (d, *J* = 9.9 Hz, 1H), 3.92 (d, *J* = 6.0 Hz, 2H). MS (EI) *m/z* 315.1 [M-H]⁻.

2.1.3.2. N-(4-(N-(4-Methoxybenzyl)sulfamoyl)phenyl)acrylamide (5b). White solid. Yield 81%. Mp 156–158 °C. ¹H NMR (300 MHz, DMSO-*d*₆) δ 10.38 (s, 1H), 7.82 (t, *J* = 6.0 Hz, 1H), 7.70 (d, *J* = 8.7 Hz, 2H), 7.61 (d, *J* = 8.7 Hz, 2H), 7.00 (d, *J* = 8.4 Hz, 4H), 6.69 (d, *J* = 8.7 Hz, 2H), 6.38–6.29 (m, 1H), 6.18 (d, *J* = 17.1 Hz, 1H), 5.69 (d, *J* = 9.9 Hz, 1H), 3.75 (d, *J* = 6.0 Hz, 2H), 3.57 (s, 3H). MS (EI) *m/z* 345.2 [M-H]⁻.

2.1.3.3. N-(4-(N-(4-Chlorobenzyl)sulfamoyl)phenyl)acrylamide (5c). White solid. Yield 80%. Mp 190–192 °C. ¹H NMR (300 MHz, DMSO-*d*₆) δ 10.40 (s, 1H), 7.98 (t, *J* = 6.3 Hz, 1H), 7.70 (d, *J* = 8.4 Hz, 2H), 7.61 (d, *J* = 8.4 Hz, 2H), 7.17 (dd, *J* = 8.4, 8.1 Hz, 4H), 6.37–6.28 (m, 1H), 6.18 (d, *J* = 16.5 Hz, 1H), 5.69 (d, *J* = 2.7 Hz, 1H), 3.82 (d, *J* = 6.0 Hz, 2H). MS (EI) *m/z* 349.1 [M-H]⁻.

2.1.3.4. N-(4-(N-(3-Chlorobenzyl)sulfamoyl)phenyl)acrylamide (5d). White solid. Yield 51%. Mp 157–159 °C. ¹H NMR (300 MHz, DMSO-*d*₆) δ 10.58 (s, 1H), 8.15 (s, 1H), 7.83 (dd, *J* = 9.0, 3.2 Hz, 2H), 7.78–7.65 (m, 2H), 7.47–7.06 (m, 4H), 6.44 (dd, *J* = 9.8, 3.4 Hz, 1H), 6.37–6.22 (m, 1H), 5.88–5.74 (m, 1H), 3.99 (d, *J* = 3.3 Hz, 2H). ¹³C NMR (126 MHz, DMSO) δ 164.08, 142.99, 140.90, 135.28, 133.36, 131.94, 130.53, 128.38, 128.13, 127.79, 127.47, 126.65, 119.53, 45.86. MS (EI) *m/z* 349.1 [M-H]⁻.

2.1.3.5. N-(4-(N-Phenethylsulfamoyl)phenyl)acrylamide (5e). White solid. Yield 75%. Mp 154–156 °C. ¹H NMR (300 MHz, DMSO-*d*₆) δ 10.39 (s, 1H), 7.70 (d, *J* = 8.1 Hz, 2H), 7.61 (d, *J* = 7.5 Hz, 2H), 7.49 (s, 1H), 7.09 (m, 4H), 6.37–6.28 (m, 1H), 6.17 (d, *J* = 15.6 Hz, 1H), 5.69 (d, *J* = 8.7 Hz, 1H), 2.80 (s, 1H), 2.53 (s, 1H). MS (EI) *m/z* 353.1 [M + Na]⁺.

2.1.3.6. N-(4-(N-(4-(Trifluoromethyl)benzyl)sulfamoyl)phenyl)acrylamide (5f). White solid. Yield 80%. Mp 198–200 °C. ¹H NMR (300 MHz, DMSO-*d*₆) δ 10.38 (s, 1H), 8.07 (s, 1H), 7.69 (d, *J* = 7.8 Hz, 2H), 7.61 (d, *J* = 8.1 Hz, 2H), 7.50 (d, *J* = 7.2 Hz, 4H), 7.33 (d, *J* = 7.2 Hz, 2H), 6.37–6.15 (m, 1H), 6.18 (d, *J* = 16.5 Hz, 1H), 5.69 (d, *J* = 9.9 Hz, 1H), 3.94 (d, *J* = 4.5 Hz, 2H). MS (EI) *m/z* 407.1 [M + Na]⁺.

2.1.3.7. N-(4-(N-(3-(Trifluoromethyl)benzyl)sulfamoyl)phenyl)acrylamide (5g). White solid. Yield 77%. Mp 152–154 °C. ¹H NMR (300 MHz, DMSO-*d*₆) δ 10.55 (s, 1H), 8.19 (t, *J* = 6.2 Hz, 1H), 7.79 (d, *J* = 8.7 Hz, 2H), 7.69 (d, *J* = 8.7 Hz, 2H), 7.55–7.44 (m, 4H), 6.49–6.40 (m, 1H), 6.27 (d, *J* = 16.8 Hz, 1H), 5.78 (d, *J* = 3.9 Hz, 1H), 4.06 (d, *J* = 6.0 Hz, 2H). MS (EI) *m/z* 383.1 [M-H]⁻.

2.1.3.8. N-(4-(N-(4-Fluorobenzyl)sulfamoyl)phenyl)acrylamide (5h). White solid. Yield 82%. Mp 178–180 °C. ¹H NMR (300 MHz, DMSO-*d*₆) δ 10.40 (s, 1H), 7.95 (t, *J* = 6.0 Hz, 1H), 7.70 (d, *J* = 8.7 Hz, 2H), 7.61 (d, *J* = 8.4 Hz, 2H), 7.14 (t, *J* = 6.8 Hz, 1H), 6.97 (t, *J* = 8.6 Hz,

2H), 6.37–6.28 (m, 1H), 6.18 (d, *J* = 17.1 Hz, 1H), 5.70 (d, *J* = 9.9 Hz, 1H), 3.82 (d, *J* = 6.0 Hz, 2H). MS (EI) *m/z* 357.1 [M + Na]⁺.

2.1.3.9. N-(4-(N-(3-Fluorobenzyl)sulfamoyl)phenyl)acrylamide (5i). White solid. Yield 80%. Mp 152–154 °C. ¹H NMR (300 MHz, DMSO-*d*₆) δ 10.39 (s, 1H), 8.01 (t, *J* = 6.3 Hz, 1H), 7.70 (d, *J* = 8.4 Hz, 2H), 7.61 (d, *J* = 5.7 Hz, 2H), 7.22–7.15 (m, 1H), 6.95–6.89 (m, 3H), 6.37–6.28 (m, 1H), 6.18 (d, *J* = 16.8 Hz, 1H), 5.69 (d, *J* = 9.9 Hz, 1H), 3.87 (d, *J* = 6.3 Hz, 2H). MS (EI) *m/z* 357.1 [M + Na]⁺.

2.1.3.10. N-(4-(N-(2-Chlorobenzyl)sulfamoyl)phenyl)acrylamide (5j). White solid. Yield 78%. Mp 178–180 °C. ¹H NMR (300 MHz, DMSO-*d*₆) δ 10.41 (s, 1H), 8.00 (s, 1H), 7.71 (d, *J* = 7.5 Hz, 2H), 7.64 (d, *J* = 8.7 Hz, 2H), 7.28–7.15 (m, 4H), 6.39–6.29 (m, 1H), 6.18 (d, *J* = 17.4 Hz, 1H), 5.69 (d, *J* = 2.7 Hz, 1H), 3.91 (d, *J* = 4.5 Hz, 2H). MS (EI) *m/z* 349.1 [M-H]⁻.

2.1.3.11. N-(4-(N-(4-Bromobenzyl)sulfamoyl)phenyl)acrylamide (5k). White solid. Yield 83%. Mp 194–196 °C. ¹H NMR (300 MHz, DMSO-*d*₆) δ 10.44 (s, 1H), 7.98 (t, *J* = 6.2 Hz, 1H), 7.71 (d, *J* = 8.4 Hz, 2H), 7.61 (d, *J* = 8.7 Hz, 2H), 7.34 (d, *J* = 7.8 Hz, 2H), 7.07 (d, *J* = 7.8 Hz, 2H), 6.38–6.29 (m, 1H), 6.17 (d, *J* = 15.9 Hz, 1H), 5.69 (d, *J* = 10.2 Hz, 1H), 3.80 (d, *J* = 6.3 Hz, 2H). MS (EI) *m/z* 393.1, 395.1 [M-H]⁻.

2.1.3.12. N-(4-(N-(3-Bromobenzyl)sulfamoyl)phenyl)acrylamide (5l). White solid. Yield 81%. Mp 156–158 °C. ¹H NMR (300 MHz, DMSO-*d*₆) δ 10.40 (s, 1H), 8.01 (t, *J* = 6.0 Hz, 1H), 7.70 (d, *J* = 8.4 Hz, 2H), 7.60 (d, *J* = 8.7 Hz, 2H), 7.26 (s, 2H), 7.11 (d, *J* = 3.9 Hz, 2H), 6.38–6.29 (m, 1H), 6.18 (d, *J* = 15.9 Hz, 1H), 5.69 (d, *J* = 10.2 Hz, 1H), 3.86 (d, *J* = 6.0 Hz, 2H). MS (EI) *m/z* 393.1, 395.1 [M-H]⁻.

2.1.3.13. N-(4-(N-(3,4-Dichlorobenzyl)sulfamoyl)phenyl)acrylamide (5m). White solid. Yield 82%. Mp 148–150 °C. ¹H NMR (300 MHz, DMSO-*d*₆) δ 10.41 (s, 1H), 8.05 (s, 1H), 7.65 (d, *J* = 29.4 Hz, 4H), 7.34 (d, *J* = 30.0 Hz, 2H), 7.11 (s, 1H), 6.38–6.15 (m, 2H), 5.70 (s, 1H), 3.82 (d, *J* = 6.0 Hz, 2H). MS (EI) *m/z* 383.1 [M-H]⁻.

2.1.4. General preparation of N-phenylacrylamide 6

To a solution of aniline (0.043 mol) in DCM (50 ml) was added TEA (0.086 mol). Then acryloyl chloride (0.047 mol) was added dropwise to the mixture at 0 °C for 0.5 h. The reaction was allowed to stir at rt overnight. After the reaction was completed, the water was added to quench the reaction. The mixture was extracted with DCM to afford the crude product that was purified by flash column chromatography on silica gel to afford N-phenylacrylamide **6** (white solid, Yield 72.8%)⁴⁰. ¹H NMR (300 MHz, Chloroform-*d*) δ 10.14 (s, 1H), 7.67 (d, *J* = 8.1 Hz, 2H), 7.32 (t, *J* = 7.8 Hz, 2H), 7.07 (t, *J* = 7.2 Hz, 1H), 6.44 (dd, *J* = 16.8, 9.9 Hz, 1H), 6.26 (dd, *J* = 16.8, 1.5 Hz, 1H), 5.75 (dd, *J* = 9.9, 1.5 Hz, 1H).

2.1.5. General preparation of 4-acrylamidobenzenesulfonyl chloride 7

N-phenylacrylamide (0.031 mol) was added slowly to sulphuryl chloride (15 ml) at 0 °C for more than 0.5 h. The reaction was stirred at 70 °C for 1 h. After the reaction was completed, the mixture was poured into ice water slowly to quench the reaction. The mixture was stirred at rt for 1 h and the solid was filtered-off and washed with water (2 × 50 ml). The crude solid was dissolved in CH₂Cl₂ (50 ml), the organic layer was washed with brine, and the

solvent was evaporated under reduced pressure to afford 4-acrylamidobenzenesulfonyl chloride as off-white solid (Yield 72.8%).

2.1.6. General preparation of compounds 8a-j

To a solution of substituted aniline or heterocyclic amine (0.98 mmol) in DCM (15 ml) was added pyridine (1.22 mmol). A solution of 4-acrylamidobenzenesulfonyl chloride (0.81 mmol) in DCM (10 ml) was added dropwise to the mixture at 0 °C. The reaction was stirred at rt for 4 h. The solvent was evaporated under reduced pressure and the crude product was recrystallization to afford target compounds **8a-j**.

2.1.6.1. N-(4-(N-Phenylsulfamoyl)phenyl)acrylamide (8a). White solid. Yield 72%. Mp 212–213 °C. ¹H NMR (300 MHz, Chloroform-d) δ 10.50 (s, 1H), 10.19 (s, 1H), 7.74 (dd, *J* = 23.7, 8.7 Hz, 4H), 7.22 (t, *J* = 7.8 Hz, 2H), 7.09–6.98 (m, 3H), 6.42 (dd, *J* = 16.8, 9.9 Hz, 1H), 6.28 (d, *J* = 15.3 Hz, 1H), 5.81 (d, *J* = 10.2 Hz, 1H). MS (EI) *m/z* 301.1 [M-H]⁻.

2.1.6.2. N-(4-(N-(p-Tolyl)sulfamoyl)phenyl)acrylamide (8b). White solid. Yield 79%. Mp 230–232 °C. ¹H NMR (300 MHz, DMSO-*d*₆) δ 10.46 (s, 1H), 9.98 (s, 1H), 7.75 (d, *J* = 8.7 Hz, 2H), 7.65 (d, *J* = 8.7 Hz, 2H), 6.96 (dd, *J* = 19.5, 8.4 Hz, 4H), 6.40 (dd, *J* = 17.1, 9.9 Hz, 1H), 6.26 (d, *J* = 17.1 Hz, 1H), 5.82–5.70 (m, 1H), 2.15 (s, 3H). MS (EI) *m/z* 315.1 [M-H]⁻.

2.1.6.3. N-(4-(N-(4-Methoxyphenyl)sulfamoyl)phenyl)acrylamide (8c). White solid. Yield 80%. Mp 234–235 °C. ¹H NMR (300 MHz, DMSO-*d*₆) δ 10.46 (s, 1H), 9.77 (s, 1H), 7.75 (d, *J* = 8.7 Hz, 2H), 7.60 (d, *J* = 8.7 Hz, 2H), 6.94 (d, *J* = 9.0 Hz, 2H), 6.77 (d, *J* = 8.7 Hz, 2H), 6.41 (dd, *J* = 17.1, 9.9 Hz, 1H), 6.26 (d, *J* = 15.3 Hz, 1H), 5.78 (d, *J* = 9.6 Hz, 1H), 3.64 (s, 3H). MS (EI) *m/z* 331.1 [M-H]⁻.

2.1.6.4. N-(4-(N-(3-Methoxyphenyl)sulfamoyl)phenyl)acrylamide (8d). White solid. Yield 77%. Mp 197–199 °C. ¹H NMR (300 MHz, DMSO-*d*₆) δ 10.38 (s, 1H), 10.09 (s, 1H), 7.63 (dd, *J* = 21.3, 8.7 Hz, 4H), 6.98 (t, *J* = 8.4 Hz, 1H), 6.53–6.51 (m, 2H), 6.45 (d, *J* = 8.4 Hz, 1H), 6.29 (dd, *J* = 16.8, 9.9 Hz, 1H), 6.15 (d, *J* = 16.8 Hz, 1H), 5.67 (d, *J* = 9.9 Hz, 1H), 3.52 (s, 3H). MS (EI) *m/z* 331.1 [M-H]⁻.

2.1.6.5. N-(4-(N-(3-Fluorophenyl)sulfamoyl)phenyl)acrylamide (8e). White solid. Yield 81%. Mp 212–215 °C. ¹H NMR (300 MHz, DMSO-*d*₆) δ 10.39–10.37 (m, 2H), 7.68 (d, *J* = 8.7 Hz, 2H), 7.60 (d, *J* = 8.7 Hz, 2H), 7.12 (t, *J* = 8.1 Hz, 1H), 6.97–6.91 (m, 3H), 6.29 (dd, *J* = 16.8, 9.6 Hz, 1H), 6.15 (d, *J* = 15.9 Hz, 1H), 5.68 (d, *J* = 9.3 Hz, 1H). MS (EI) *m/z* 319.1 [M-H]⁻.

2.1.6.6. N-(4-(N-(3-Chlorophenyl)sulfamoyl)phenyl)acrylamide (8f). White solid. Yield 83%. Mp 217–219 °C. ¹H NMR (300 MHz, DMSO-*d*₆) δ 10.39 (d, *J* = 8.1 Hz, 2H), 7.69 (d, *J* = 9.0 Hz, 2H), 7.61 (d, *J* = 9.0 Hz, 2H), 7.12 (t, *J* = 7.8 Hz, 1H), 6.97–6.92 (m, 3H), 6.30 (dd, *J* = 17.1, 10.2 Hz, 1H), 6.16 (d, *J* = 16.8 Hz, 1H), 5.70–5.62 (m, 1H). MS (EI) *m/z* 335.1 [M-H]⁻.

2.1.6.7. N-(4-(N-(3-Chloro-4-fluorophenyl)sulfamoyl)phenyl)acrylamide (8g). White solid. Yield 70%. Mp 224–226 °C. ¹H NMR (300 MHz, DMSO-*d*₆) δ 10.42 (s, 1H), 7.66 (d, *J* = 8.7 Hz, 2H), 7.56 (d, *J* = 8.4 Hz, 2H), 7.16 (t, *J* = 9.1 Hz, 1H), 7.05 (d, *J* = 4.5 Hz, 1H), 6.93–6.89 (m, 1H), 6.28 (dd, *J* = 16.5, 9.6 Hz, 1H), 6.15 (d, *J* = 16.8 Hz, 1H), 5.68 (d, *J* = 9.6 Hz, 2H). ¹³C NMR (126 MHz, DMSO) δ 164.19, 154.52 (d, *J*_{C-F} = 244.44 Hz, 1C), 143.66, 135.54, 133.30,

128.44, 128.38, 122.42, 121.28, 121.22, 120.13 (d, *J*_{C-F} = 6.3 Hz, 1C), 119.60, 117.90 (d, *J*_{C-F} = 22.68 Hz, 1C). MS (EI) *m/z* 353.1 [M-H]⁻.

2.1.6.8. N-(4-(N-(Pyrimidin-2-yl)sulfamoyl)phenyl)acrylamide (8h). White solid. Yield 70%. Mp 229–230 °C. ¹H NMR (300 MHz, DMSO-*d*₆) δ 11.73 (s, 1H), 10.52 (s, 1H), 8.50 (d, *J* = 4.9 Hz, 2H), 7.95 (d, *J* = 9.0 Hz, 2H), 7.93 (d, *J* = 8.7 Hz, 2H), 7.05 (t, *J* = 4.9 Hz, 1H), 6.45 (dd, *J* = 17.0, 9.9 Hz, 1H), 6.30 (dd, *J* = 16.9, 2.1 Hz, 1H), 5.82 (dd, *J* = 9.8, 2.0 Hz, 1H). MS (EI) *m/z* 327.1 [M + Na]⁺.

2.1.6.9. N-(4-(N-(3,4-Dimethylisoxazol-5-yl)sulfamoyl)phenyl)acrylamide (8i). White solid. Yield 81%. Mp 206–208 °C. ¹H NMR (300 MHz, DMSO-*d*₆) δ 10.96 (s, 1H), 10.61 (s, 1H), 7.89–7.86 (d, *J* = 9.0 Hz, 2H), 7.74–7.71 (d, *J* = 9.0 Hz, 2H), 6.51–6.42 (m, 1H), 6.34–6.29 (d, *J* = 15.0 Hz, 1H), 5.85–5.82 (d, *J* = 9.0 Hz, 1H), 2.08 (s, 3H), 1.63 (s, 3H). MS (EI) *m/z* 320.1 [M-H]⁻.

2.1.6.10. N-(4-(N-(5-Methylisoxazol-3-yl)sulfamoyl)phenyl)acrylamide (8j). White solid. Yield 85%. Mp 232–233 °C. ¹H-NMR (300 MHz, DMSO-*d*₆) δ 11.35 (s, 1H), 10.56 (s, 1H), 7.87–7.80 (dd, *J* = 12.0, 9.0 Hz, 4H), 6.49–6.40 (m, 1H), 6.33–6.28 (d, *J* = 15.0 Hz, 1H), 6.13 (s, 1H), 5.85–5.81 (dd, *J* = 9.0, 3.0 Hz, 1H), 2.29 (s, 3H). MS (EI) *m/z* 306.1 [M-H]⁻.

2.2. Biological assays

The main bioassays performed in the study, including HeLa cell-based IDO1/kynurenine assay, Western blot analysis, T cell proliferation and Treg cell differentiation experiments, were carried out as described previously³².

2.2.1. Cellular thermal shift assay

HeLa cells were seeded in 6-well culture plates at a density of 2×10^5 per well. On the next day, human IFN- γ (100 ng/mL) were added and incubated for 24 h, and then the cells were treated with **5d** for 2 h. At the end of incubation, cells collected and subjected to CETSA assay. Briefly, incubated cells were equally divided into 10 parts, each part was heated for 3 min under different temperature (43, 46, 49, 52, 55, 58, 61, 64, 67, and 70 °C), and then the heated cells were kept at -80 °C for 12 h, then at room temperature for 5 min, and the process repeated one more time. After that, cell lysates were extracted by centrifugation at 20,000 \times g, 20 min. Levels of IDO1 protein were assessed by Western blot analysis.

2.2.2. In vivo antitumour activity assay

BALB/c mice (6–8 weeks old, 18–22 g) were supplied by Model Animal Research Centre of Nanjing University (Nanjing, China). Mice were maintained under standard specific-pathogen-free (SPF) conditions (21 \pm 2 °C and 12-h light: dark cycle). Animal welfare and experimental procedures were carried out strictly in accordance with the Guide for the Care and Use of Laboratory Animals (The Ministry of Science and Technology of China, 2006) and the related ethical regulations of our university. All efforts were made to minimise animals' suffering and to reduce the number of animals used. Mouse colon cancer cells (CT26) and melanoma cells (B16F1) were cultured and collected by centrifugation (1000 rpm, 5 min) and washed twice with ice-cold PBS. Then cells were diluted to 1×10^7 /ml and 1×10^6 CT26/B16F1 cells (in 0.1 ml PBS)

were injected subcutaneously into the right flanks of mice. All mice formed tumours three days after injection. Then mice were randomly distributed into five groups ($n=10/8$) according to tumour volumes. **5d** (3.125, 6.5, 12.5 mg/kg) were administered (i.g) to each group respectively every day. 5-FU (25 mg/kg) and Cis-platinum (1 mg/kg) were administered (i.p) every three days. Tumour length and tumour width were measured with a Vernier calliper every three days. Tumour volumes were measured and calculated using the equation $\text{volume} = a \times b^2/2$, where "a" is the maximal width and "b" is maximal orthogonal width. After the administration were completed, mice were weighed, euthanized, and tumours were removed and the weight were taken.

Eight-week-old male BALB/c nude mice, weighing 18–22 g, were supplied by Model Animal Research Centre of Nanjing University (Nanjing, China). $1 \times 10^7/\text{ml}$ and 1×10^6 CT26 cells (in 0.1 ml PBS) were injected subcutaneously into the right flanks of mice. After CT26 xenograft BALB/c nude mouse model was established, all mice were randomly divided into three groups ($n=8$). **5d** (12.5 mg/kg) were administered (i.g) every day and 5-FU (25 mg/kg) were administered (i.p) every three days. The following experimental procedures were similar to the described above.

2.2.3. Immunohistochemistry analysis

For immunohistochemistry staining, the sections were deparaffinized, rehydrated, and washed in 1% PBS-Tween 20, and then treated with 2% hydrogen peroxide, blocked with 3% goat serum (Life Technology, 16210–064) and incubated for 2 h at room temperature with specific primary antibodies. Then the slides were incubated with streptavidin-HRP (Shanghai Gene Company, GK500705) for 40 min, then stained with DAB (Shanghai Gene Company, GK500705) substrate and counter-stained with haematoxylin. Images were acquired by microscopy (Olympus IX51).

2.3. Molecular modelling

In order to consider the flexibility of both ligand and protein, the induced fit docking (IFD) protocol in Schrödinger was employed.

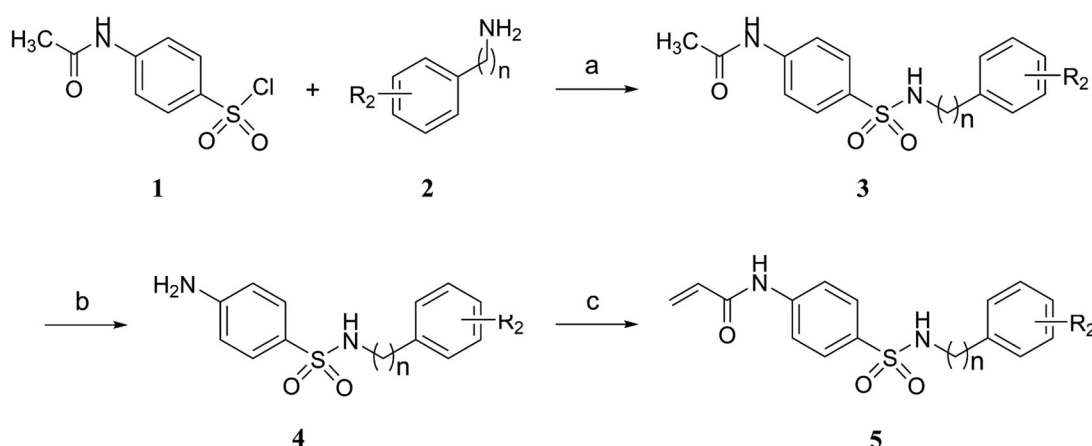
In IFD calculations, the ligands were first docked into the rigid receptor using softened energy function in *Glide*. By default, a maximum 20 poses per ligand were retained. Then, the protein degrees of freedom for each complex were sampled and the protein-ligand complexes were minimised. The protein structure in each pose now reflected an induced fit to the ligand structure and conformation. The best protein-ligand complex was then identified based on the predicted binding affinities of the docked ligand. Here, the residues within 5 Å of each of the 20 ligand poses were subjected to a conformational search and energy minimizations, and the residues outside this range were fixed. Finally, the minimised ligand was rigorously redocked into the induced-fit protein structure using *Glide* XP scoring mode, and metal constraints can be applied to both *Glide* docking stages in IFD protocol. The choice of the best-docked structure for each ligand was made using a model energy score that combines the energy grid score, the binding affinity predicted by *GlideScore*, and the internal strain energy for the model potential used to direct the conformational-search algorithm.

3. Results and discussion

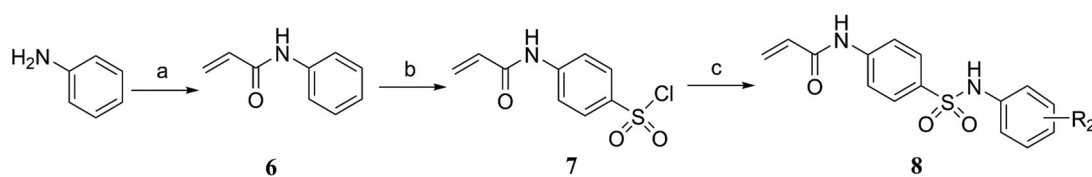
3.1. Chemistry

The synthetic pathways for the target compounds were shown in *Scheme 1* and *2*. *N*-acetyl secondary sulphonamides **3** were prepared by the condensation reaction of substituted 4-acetamidobenzenesulfonyl chloride **1** with various amines **2**. Deacetylation of compounds **3** with concentrated HCl in ethanol gave amino secondary sulphonamides hydrochloride salts, and followed by neutralisation with saturated NaHCO_3 solution to afford the corresponding amino secondary sulphonamides **4**. Finally, the compounds **5** were prepared via the condensation reaction of compounds **4** with acryloyl chloride (*Scheme 1*).

Alternatively, *N*-phenylacrylamide **6** was synthesised by condensation of aniline with acryloyl chloride in the presence of triethylamine, and followed by chlorosulfonation with chlorosulfonic acid to give 4-acetamidobenzenesulfonyl chloride **7**. Subsequently,



Scheme 1. Reagents and conditions: (a) TEA, DCM, 0 °C, rt; (b) HCl, ethanol, 70 °C; (c) Acryloyl chloride, TEA, DCM, 0 °C, rt.



Scheme 2. Reagents and conditions: (a) Acryloyl chloride, TEA, DCM, 0 °C, rt; (b) HSO_3Cl , 70 °C, 1 h; (c) Substituted aniline, pyridine, DCM, 0 °C, rt.

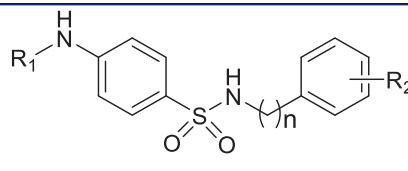
the 4-acetamidobenzenesulfonyl chloride was treated with substituted aniline in the presence of pyridine to form the target compounds **8** (Scheme 2).

3.2. Effect of secondary sulphonamides on IDO1 activity

It is well known that IDO1 is broadly expressed in human cancers and is induced by pro-inflammatory cytokines, such as interferon gamma (IFN- γ) and tumour necrosis factor alpha (TNF- α)⁴¹. Here we utilised a human cervical cancer cell line HeLa that endogenously expresses IDO1 upon IFN- γ treatment to evaluate the IDO1 inhibitory activity of the synthesised compounds by measuring kynurenine secreted into the media. This cell-based assay, as a rapid and simple method for determination IDO1/kynurenine, is closely related to the potency of the enzyme assay and has been widely used to identify various IDO1 inhibitors^{19,23,29,42}. In addition, cytotoxic compounds can reduce cell viability, which will decrease the IDO1 levels and then lower the conversion of tryptophan to kynurenine. Thus, we also employed this cellular assay to detect false positive IDO1 inhibitors and cytotoxic compounds by measuring HeLa cell viability. Clinical candidate navoximod was used as an assay control. The results were shown in Table 1 and 2.

Our group had already synthesised a series of *N*-acetyl secondary sulphonamides as the analogs of compound BS-1 and evaluated their inhibitory activity⁴³. To our surprise, although most of these compounds had weak inhibitory activity against IDO1, *N*-(4-(*N*-(4-methoxybenzyl)sulfamoyl)phenyl)acetamide (HeLa IC₅₀: 5.88 μ M) showed good inhibitory activity, and its potency was

Table 1. IDO1 inhibitory activity of the target compounds **3a-i**, **4a-f**, **5a-e** and **8a-b**.



Compd.	R ₁	n	R ₂	Inhibition %*	IC ₅₀ (μ M)
BS-1	CH ₃ CO	1	<i>m</i> -Cl	30.7%	49.42
3a	CH ₃ CO	0	H	3.9%	N.D.**
3b	CH ₃ CO	0	<i>p</i> -CH ₃	16.3%	N.D.
3c	CH ₃ CO	0	<i>p</i> -CH(CH ₃) ₂	5.9%	N.D.
3d	CH ₃ CO	0	<i>m</i> -CH(CH ₃) ₂	14.6%	N.D.
3e	CH ₃ CO	1	H	2.5%	N.D.
3f	CH ₃ CO	1	<i>p</i> -Cl	13.5%	N.D.
3g	CH ₃ CO	1	<i>p</i> -CF ₃	14.5%	N.D.
3h	CH ₃ CO	1	<i>m</i> -CF ₃	7.8%	N.D.
3i	CH ₃ CO	2	H	5.9%	N.D.
4a	NH	0	H	12.0%	N.D.
4b	NH	0	<i>p</i> -CH ₃	10.8%	N.D.
4c	NH	1	H	7.4%	N.D.
4d	NH	1	<i>p</i> -Cl	-4.2%	N.D.
4e	NH	1	<i>m</i> -Cl	2.3%	N.D.
4f	NH	2	H	3.1%	N.D.
5a	CH ₂ =CHCO	1	H	62.5%	22.36
5b	CH ₂ =CHCO	1	<i>p</i> -OCH ₃	36.0%	40.06
5c	CH ₂ =CHCO	1	<i>p</i> -Cl	40.4%	36.20
5d	CH ₂ =CHCO	1	<i>m</i> -Cl	91.1%	6.26
5e	CH ₂ =CHCO	2	H	55.2%	26.27
8a	CH ₂ =CHCO	0	H	85.9%	13.18
8b	CH ₂ =CHCO	0	<i>p</i> -CH ₃	25.3%	N.D.
Navoximod				98.6%	0.41

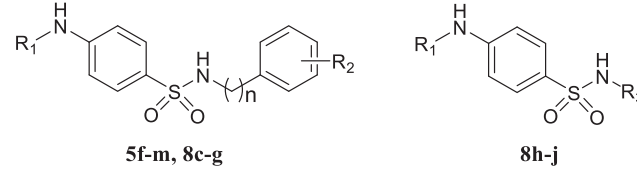
*Percentage inhibition at 30 μ M.

**N.D.: not determined.

remarkably increased by 8.4-fold as compared with the hit BS-1. Inspired by *N*-(4-(*N*-(4-methoxybenzyl)sulfamoyl)phenyl)acetamide, we further synthesised the analogues **3a-i** bearing an electron-donor group on the benzyl group, but they displayed only weak activity. Subsequently, we tried to remove the acetyl group of *N*-acetyl secondary sulphonamides, and found that all the obtained aniline compounds **4a-f** had no improvement in activity. These results indicated that a free amino group on the phenyl ring with strong electron-donating ability appeared to be unfavourable for the inhibitory activity of these compounds. To this end, we tried to introduce an acryloyl group instead of the acetyl group to the amine group. As expected, compounds **5a-e** bearing an acetyl group showed moderate to good inhibitory activity. Especially, compound **5d** (HeLa IC₅₀: 6.26 μ M) exhibited significantly stronger activity than the hit compound BS-1 (HeLa IC₅₀: 49.42 μ M) and its corresponding acetyl compound **4e** (HeLa IC₅₀ > 50 μ M).

We then further optimised the inhibitory activity of *N*-acryloyl secondary sulphonamides by modifying the substituents, including *n*, R₂ and R₃, while retaining the acryloyl group at R₁. As shown in Table 2, most of *N*-acryloyl secondary sulphonamides displayed good inhibitory activity against IDO1. Among them, benzylamine derivative **5l** and aniline derivative **8g** exhibited potent activity with IC₅₀ values of 6.64 μ M and 3.76 μ M, which were significantly increased by 7.4-fold and 13.1-fold as compared with the hit BS-1, respectively. It is worth noting that the compounds **5d**, **5g**, **5l**, and **8d** with a substituent at 3-position on aniline or benzylamine had higher activity than those compounds **5c**, **5f**, **5k** and **8c** with a substituent at 4-position (**5c** vs **5d**, **5f** vs **5g**, **5k** vs **5l**, **8c** vs **8d**). However, compound **5i** (IC₅₀: 39.53 μ M) with a fluoro substituent

Table 2. IDO1 inhibitory activity of the target compounds **5f-m** and **8c-j**.



Compd.	R ₁	n	R ₂	R ₃	Inhibition %*	IC ₅₀ (μ M)
5f	CH ₂ =CHCO	1	<i>p</i> -CF ₃	-	38.2%	39.16
5g	CH ₂ =CHCO	1	<i>m</i> -CF ₃	-	49.5%	30.53
5h	CH ₂ =CHCO	1	<i>p</i> -F	-	70.9%	20.54
5i	CH ₂ =CHCO	1	<i>m</i> -F	-	37.8%	39.53
5j	CH ₂ =CHCO	1	<i>o</i> -Cl	-	65.1%	22.66
5k	CH ₂ =CHCO	1	<i>p</i> -Br	-	37.5%	42.08
5l	CH ₂ =CHCO	1	<i>m</i> -Br	-	89.1%	6.64
5m	CH ₂ =CHCO	1	<i>m,p</i> -diCl	-	44.0%	37.27
8c	CH ₂ =CHCO	0	<i>p</i> -OCH ₃	-	20.9%	N.D.**
8d	CH ₂ =CHCO	0	<i>m</i> -OCH ₃	-	74.8%	13.45
8e	CH ₂ =CHCO	0	<i>m</i> -F	-	69.7%	17.66
8f	CH ₂ =CHCO	0	<i>m</i> -Cl	-	89.5%	9.48
8g	CH ₂ =CHCO	0	<i>m</i> -Cl- <i>p</i> -F	-	93.2%	3.76
8h	CH ₂ =CHCO	0	-	-	16.4%	N.D.
8i	CH ₂ =CHCO	0	-	-	23.6%	N.D.
8j	CH ₂ =CHCO	0	-	-	22.7%	N.D.
Navoximod					98.6%	0.41

*Percentage inhibition at 30 μ M.

**N.D.: not determined.

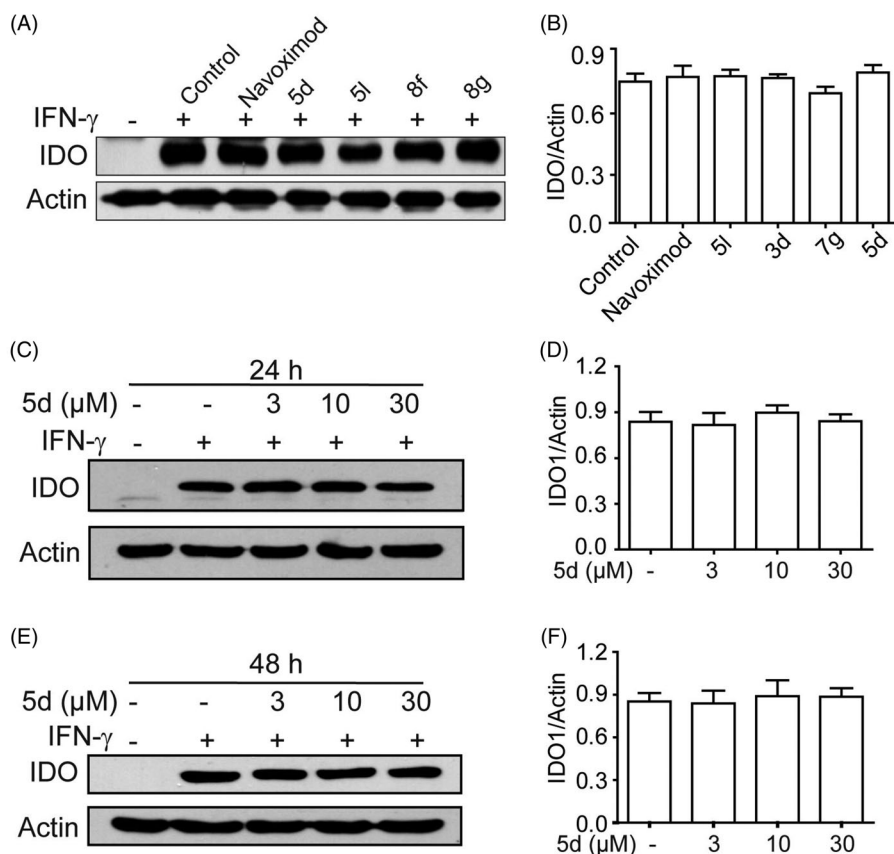


Figure 3. Compounds **3d**, **5d**, **5l** and **8g** did not affect the expression of IDO1 protein. (A) HeLa cells were treated with IFN- γ (100 ng/mL) for 24 h, then incubated with or without test compounds at their IC₅₀ concentrations for 24 h, and expression of IDO was analysed by Western blot using an anti-IDO antibody. (B) The greyscale scanning statistical results of A. (C) HeLa cells were incubated with compound **5d** (3, 10, 30 μ M) for 24 h. (D) The greyscale scanning statistical results of C. (E) HeLa cells were incubated with compound **5d** (3, 10, 30 μ M) for 48 h. (F) The greyscale scanning statistical results of E. Data are presented as means \pm SEM ($n=3$).

at 3-position on aniline showed lower inhibitory activity compared with the corresponding compound **5h** with a fluorine atom at 4-position on aniline (IC₅₀: 20.54 μ M), which showed similar inhibitory activity with compound **5a** without substituent on aniline (IC₅₀: 22.36 μ M), likely due to the similar size of the fluorine and hydrogen atoms. Interestingly, compound **8g** containing a *m*-chlorine and a *p*-fluorine atoms showed the strongest potency (IC₅₀: 3.76 μ M), while compound **5m** with *m,p*-di-chlorine atoms had only moderate activity (IC₅₀: 37.27 μ M). It might be due to the large volume of the 4-substituent on aniline or benzylamine that cause the bad clashes with the neighbouring residues in active site of IDO1. In addition, we also tried to replace benzene or benzyl rings with aromatic heterocycles (**8h-8j**), including pyrimidine and isoxazole, but they showed only weak activity.

Taken together, compounds **5d**, **5l** and **8g** showed good inhibitory activity in the HeLa cell-based IDO1/kynurenine assay. Furthermore, the viability of HeLa cells was evaluated by the MTT method at the end of the assay. The readouts showed that most of the synthesised compounds did not affect cell viability under the experimental conditions (data not shown), indicating that IDO1 inhibitory activity of these compounds is not mediated by their cytotoxicity.

3.3. Effect of 5d, 5l, 8f and 8g on IDO1 protein expression

To exclude the possibility that these secondary sulphonamides inhibit IDO1 activity by down-regulating IDO1 expression, we utilised Western blot to measure the expression of IDO1 protein in HeLa cells treated with different compounds. As depicted in

Figure 3, compared with the blank group, the expression of IDO1 protein was significantly induced in IFN- γ -treated HeLa cells. Evidently, all tested compounds **5d**, **5l**, **8f** and **8g** did not influence IDO1 expression as compared with the control group. In addition, we further confirmed that treatment of HeLa cells with different concentrations of compound **5d** (3, 10, 30 μ M) for 24 h or 48 h also did not affect IDO1 expression. The results demonstrated that these compounds blocked the kynurenine pathway by affecting IDO1 enzyme activity rather than its expression and/or HeLa cell viability.

3.4. Compounds 5d and 8g could effectively restore T cell proliferation

T lymphocytes are exceedingly sensitive to low tryptophan levels. Overactivation of the kynurenine pathway by high IDO1 expression leads to local tryptophan depletion, which can suppress T cell proliferation by activating the GCN2 kinase pathway and eventually result in T cell anergy⁴⁴. Here, to determine whether secondary sulphonamides could rescue IDO1-mediated blockade of T cell proliferation, we used a co-culture of IDO1-expressing B16F1 melanoma cells with naïve CD4⁺ T cells to mimic the tumour microenvironment. Given that melanoma is a highly immunogenic tumour and IDO1 constitutively expresses in melanoma cells⁴⁰, B16F1 murine melanoma cell lines that express IDO1 were then used to co-culture with T cells. Naïve CD4⁺ T cells were isolated from spleens of C57BL/6 mice. As shown in Figure 4, compounds **5d**, **8g** and navoximod displayed a significant augmentation on T cell activity stimulated with B16F1 cells. Especially,

compound **5d** showed better enhancement of T cell proliferation than navoximod. These findings demonstrated that compounds **5d** and **8g** could reverse the suppression of T lymphocytes caused by IDO1.

3.5. Compounds **5d** and **8g** could effectively inhibit FoxP3⁺ Treg cell differentiation

Besides causing local tryptophan depletion, high IDO1 expression can also accumulate metabolites of kynurenine pathway. The elevated metabolites can not only induce effector T cell death directly through their cytotoxicity, but also promote the differentiation of naïve CD4⁺ T cells into CD4⁺ FoxP3⁺ Treg cells by activating the AHR pathway¹⁰. As a highly immunosuppressive subset of CD4⁺ T cells, FoxP3⁺ Treg cells are critical to the maintenance of immune homeostasis and are involved in tumour immune escape, thereby contributing to tumour development and progression⁴⁵. Therefore, we also utilised co-culture of B16F1 cells with naïve CD4⁺ T cells to test whether the synthesised compounds could suppress IDO1 mediated Treg cell differentiation. As illustrated in Figure 5, when the naïve CD4⁺ T cells were co-cultured with B16F1 cells under Con A stimulation for 48 h, the

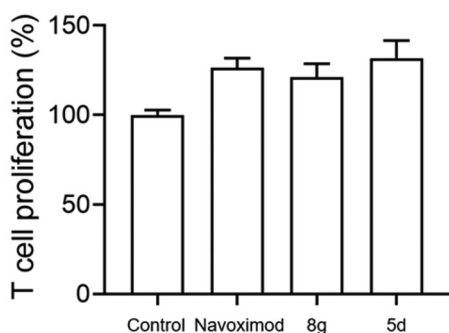
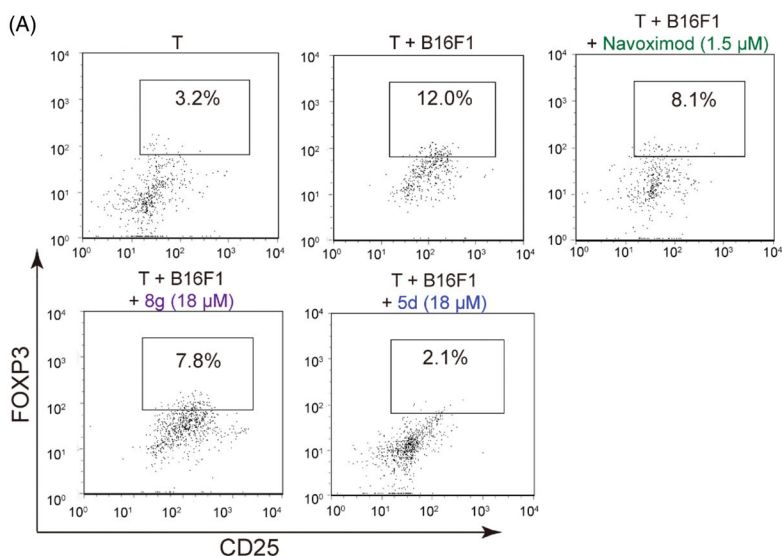


Figure 4. Compounds **5d** and **8g** could promote the proliferation of T cells. Based on the B16F1-T cell co-culture system, use MTT assay to test T cells proliferation. The Navoximod and compounds were added to the system at the concentration of 1.5 and 18 μ M. Data represent mean \pm SEM ($n = 3$).



(B)

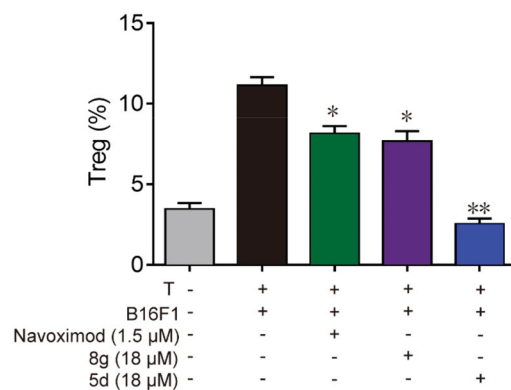


Figure 5. Compounds **5d** and **8g** inhibited Treg cell differentiation in the cell co-culture system. (A) After co-cultured with B16F1 cells, T cells were collected. Surface staining was performed with CD4⁺ FITC and CD25⁺ PE for 30 min at 4 °C. The cells were fixed and permeabilized with fixation buffer and permeabilization wash buffer. The intracellular staining was performed with FoxP3⁺ APC for 20 min. The cells were then analysed by flow cytometry analysis. (B) Statistical analysis of result A. Data are represented as \pm SEM ($n = 3$). * $p < 0.05$, ** $p < 0.01$ vs T + B16F1.

number of the FoxP3⁺ Treg cells increased approximately 4 times compared with naïve T cells cultured alone, indicating that IDO1-expressing B16F1 cells could significantly stimulate naïve T cell differentiation into FoxP3⁺ Treg cells. However, treatment with **5d**, **8g** and navoximod could significantly reduce FoxP3⁺ Treg cell differentiation. Especially, compound **5d** displayed the best effect in this test, and its FoxP3⁺ Treg cell number returned to the initial level. These data evidenced that compounds **5d** and **8g** could effectively suppress the differentiation of naïve CD4⁺ T cell into FoxP3⁺ Treg cells, which would help reverse IDO1-mediated immune suppression.

3.6. Compound **5d** could bind to IDO1 protein in HeLa cells

The cellular thermal shift assay (CETSA) is usually used to identify compounds and their potential targets. CETSA can detect the target engagement of drugs in a cellular context based on the biophysical principle of ligand-induced thermal stabilisation of target proteins⁴⁶. To this end, we further employed the CETSA assay to detect whether compound **5d** could directly bind to the target protein IDO1 in HeLa cells. As presented in Figure 6, treatment with **5d** could improve the thermal stability of IDO1 protein in HeLa cells as compared with the vehicle control, and still maintained the protein stability at 55 °C. These results suggested that compound **5d** could enter HeLa cells and then directly bind to IDO1 protein.

3.7. Compound **5d** could effectively inhibit colon carcinoma growth in immunocompetent mice, but not in immunodeficient mice

Given that it was the most prominent inhibitor *in vitro*, we chose compound **5d** for further pharmacodynamic evaluation *in vivo*. Bowel cancer is the third leading cause of cancer in the world, thus we first evaluated the efficacy of compound **5d** on the growth of murine CT26 colon carcinoma xenograft model in immunocompetent BALB/c mice. Fluorouracil (5-FU) is one of the most commonly used drugs to different cancers including bowel cancer, and was used as the positive control. The CT26 tumour-

bearing mice were treated with **5d** (3.125, 6.25, 12.5 mg/kg, i.g, every day) or 5-FU (25 mg/kg, i.p, every other day). Tumour volumes were measured every two days for 14 days. As outlined in Figure 7, treatment of **5d** significantly suppressed the growth of tumour in a dose-dependent manner as compared with the vehicle group. Especially, **5d** reduced tumour volume by 35.9% and average tumour weight by 37.5% at the dose of 12.5 mg/kg, which were comparable to that of 5-FU. Moreover, no significant change in body weight of the mice was observed in administration groups compared with the vehicle group during the 14-day treatment.

Then, in order to clarify whether the *in vivo* antitumour efficacy of compound **5d** was related to the mouse immune system, we repeated the above experiment in immunodeficient nude mice. Briefly, BALB/c nude mice bearing established CT26 colon

carcinoma xenograft were treated with compound **5d** and 5-FU for 10 days. As introduced in Figure 8, administration of **5d** did not block tumour growth as compared with the vehicle group, while classical cytotoxics 5-FU significantly suppressed tumour growth. Taken together, these results implied that the *in vivo* anti-tumour efficacy of compound **5d** was achieved by activating mouse immune system rather than its cytotoxicity.

3.8. Compound 5d could inhibit the growth of tumour cells by curbing proliferation and inducing apoptosis in CT26 tumour tissues

In order to further observe morphological changes in tumour tissues after administration of compound **5d**, the tumour tissue sections obtained from the BALB/c mice bearing CT26 colorectal tumours were stained with haematoxylin-eosin (H&E) to highlight different tissue structures, such as the nucleus and cytoplasm. As illustrated in Figure 9(A), the number of tumour cells in 5-FU-treated group was significantly reduced as compared with the vehicle group. Similarly, administration of **5d** decreased the number of tumour cells, as well as led to the morphological changes including cell shrinkage and chromatin condensation in a dose-dependent manner. In addition, it was clearly observed from the enlarged local image that there are more blood vessels in the compound **5d** group, and their morphology appears more normal, suggesting that compound **5d** might contribute to tumour vascular normalisation, thereby promoting antitumour effect of the immune system⁴⁷.

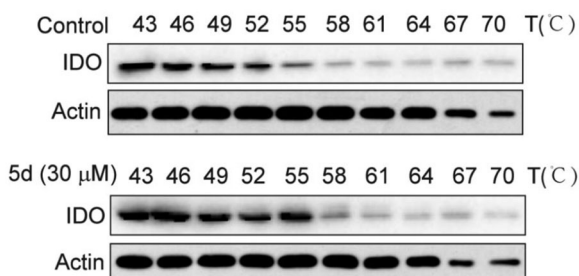


Figure 6. Compound **5d** could bind to IDO1 protein in HeLa cells. HeLa cells were treated with human IFN- γ (100 ng/mL) for 24 h, and then treated with **5d** for 2 h. The cells were collected and subjected to CETSA assay. The levels of IDO1 protein were assessed by Western blot analysis.

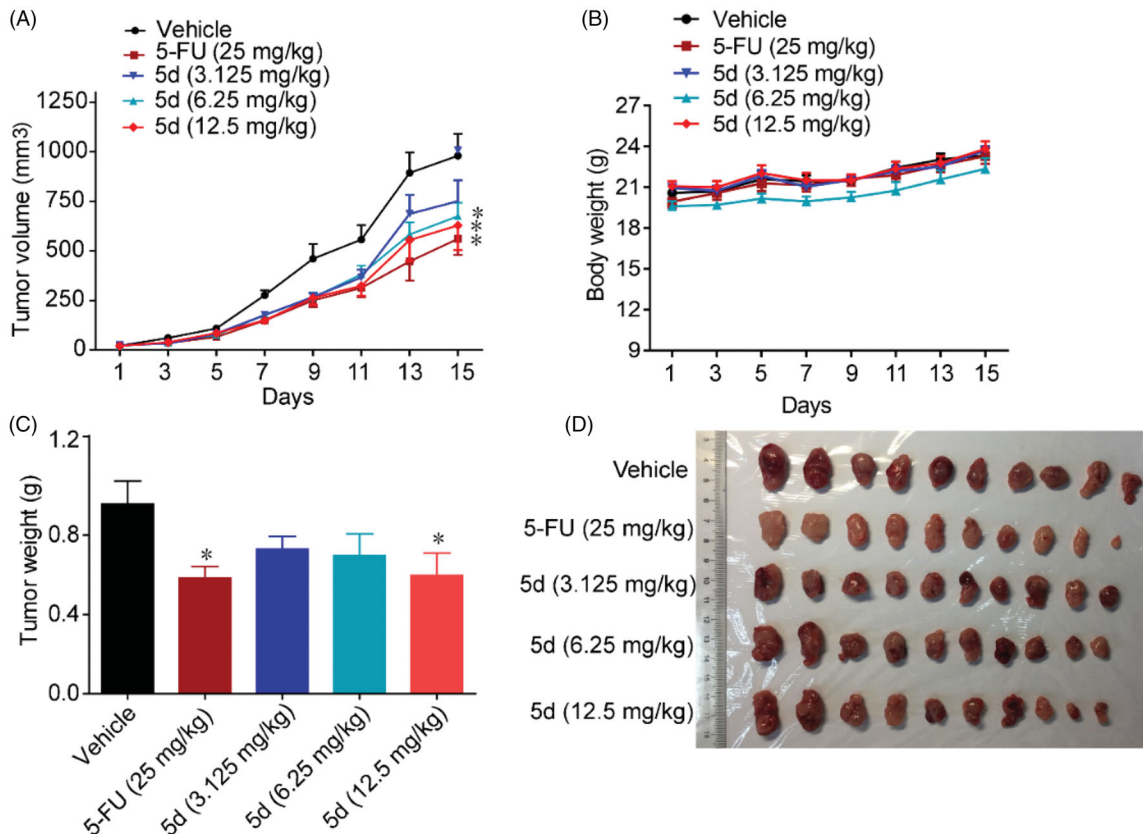


Figure 7. Compound **5d** suppressed colon cancer growth in immunocompetent mice. 1×10^6 CT26 cells were transplanted subcutaneously into the armpit of the BALB/c mice. Three days after transplantation, mice were randomly allocated to vehicle control or treatment groups ($n=10$). Drugs were administered on days 1–14. Tumour volume (A) and mice body weight (B) were recorded. After sacrifice, solid tumours were separated and weighed (C, D). Data represent mean \pm SEM, $n=10$, * $p < 0.05$, ** $p < 0.01$ vs vehicle.

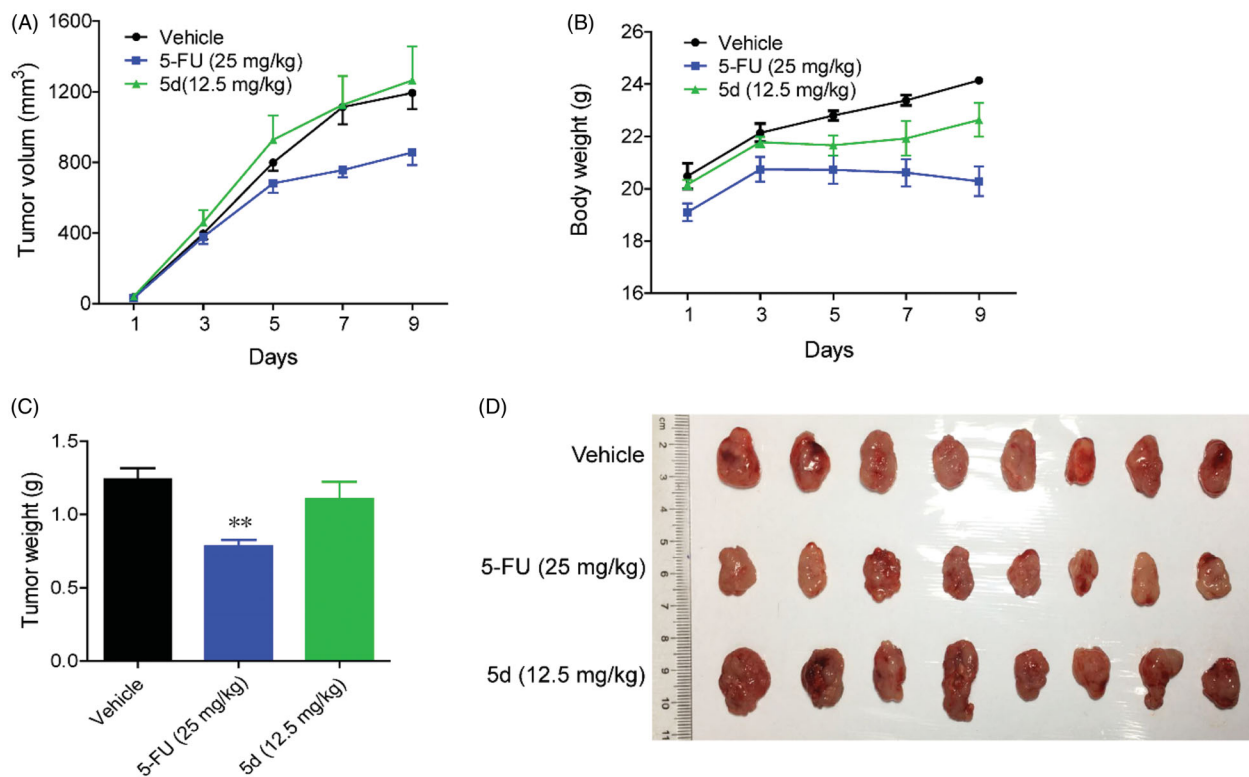


Figure 8. Compound **5d** did not suppress the growth of CT26 tumour in nude mice. 1×10^6 CT26 cells were transplanted subcutaneously into the armpit of immunodeficient BALB/c nude mice. Three days after transplantation, mice were randomly allocated to vehicle control or treatment groups ($n = 8$). Drugs were administered on days 1–9. (A) Tumour volume and mouse body weight (B) were recorded. After sacrifice, solid tumours were separated and weighed (C, D). Data represent mean \pm SEM, $n = 8$, * $p < 0.05$, ** $p < 0.01$ vs vehicle.

Then, to understand the mechanism of tumour cell death, we detected the level of proliferating cell nuclear antigen (PCNA) protein and tumour cell apoptosis by immunohistochemistry (IHC) and terminal deoxynucleotidyl transferase dUTP nick end labelling (TUNEL) experiments, respectively. PCNA is known as a molecular marker for assessing cell proliferation status, and TUNEL assay is the most widely used method to identify apoptotic cells. The results of IHC analysis showed that the expression of PCNA protein in the 5-FU group was significantly reduced as compared with the vehicle group. The similar results were observed in the **5d** treatment group and showed a dose-response relationship (Figure 9(B)). In addition, the results of TUNEL assay showed that the tumour cells had less apoptosis in the vehicle group, while the apoptosis increased in the 5-FU group. Likewise, treatment with **5d** also significantly induced the tumour cell apoptosis in a dose-dependent manner (Figure 9(C)). These data revealed that compound **5d** displayed *in vivo* antitumour efficacy by inhibiting tumour cell proliferation and inducing apoptosis.

To verify the above conclusions, we further performed H&E and IHC staining on the nude mouse CT26 tumour tissues. As depicted in Figure 10(A), the tumour cells in the **5d**-treated group remained intact morphology and were arranged in an orderly manner as that in the vehicle-treated group, while the results of 5-FU treatment were just the opposite. Moreover, the results of TUNEL assay showed that administration of **5d** had no influence on the expression of PCNA (Figure 10(B)). These findings further supported the above conclusions.

3.9. Compound **5d** facilitated immune system rejuvenation in CT26 tumour-bearing mice

To investigate the effect of compound **5d** on the immune function in CT26 tumour-bearing mice, we carried out the IHC experiment to detect the expression of IFN- γ and granzyme B in the tumour tissues. IFN- γ is a key cytokine secreted primarily by activated T cells and NK cells, which is essential for both innate and adaptive immunity. Therefore, IFN- γ is an important sign of rejuvenation of the immune system. Moreover, cytotoxic T lymphocytes (CTLs) is the key effector cells of the adaptive antitumour immune response. Granzyme B is the primary mediator of apoptosis by CTLs and NK cells. It can initiate the processing of caspases and apoptosis when it is released from activated CTLs⁴⁸. As detailed in Figure 11, compared with the vehicle, administration of compound **5d** increased the expression of IFN- γ in a dose-dependent manner in the CT26 tumour tissues, suggesting that **5d** treatment could facilitate T cell activation and the rejuvenation of the immune system in the tumour microenvironment. Similarly, all treatments of **5d** elevated granzyme B levels, which was consistent with the results of the TUNEL assay described above.

Furthermore, we also detected the content of FoxP3⁺ Treg cells in the CT26 tumour-bearing mouse spleens by fluorescence activated cell sorting (FACS) assay (Figure 12). The results showed that **5d** treatment decreased the number of FoxP3⁺ Treg cells in a dose-dependent manner. Especially, the amount in the high dose group was reduced 2.4-fold compared with the vehicle group. Taken together, these results revealed that the compound **5d**

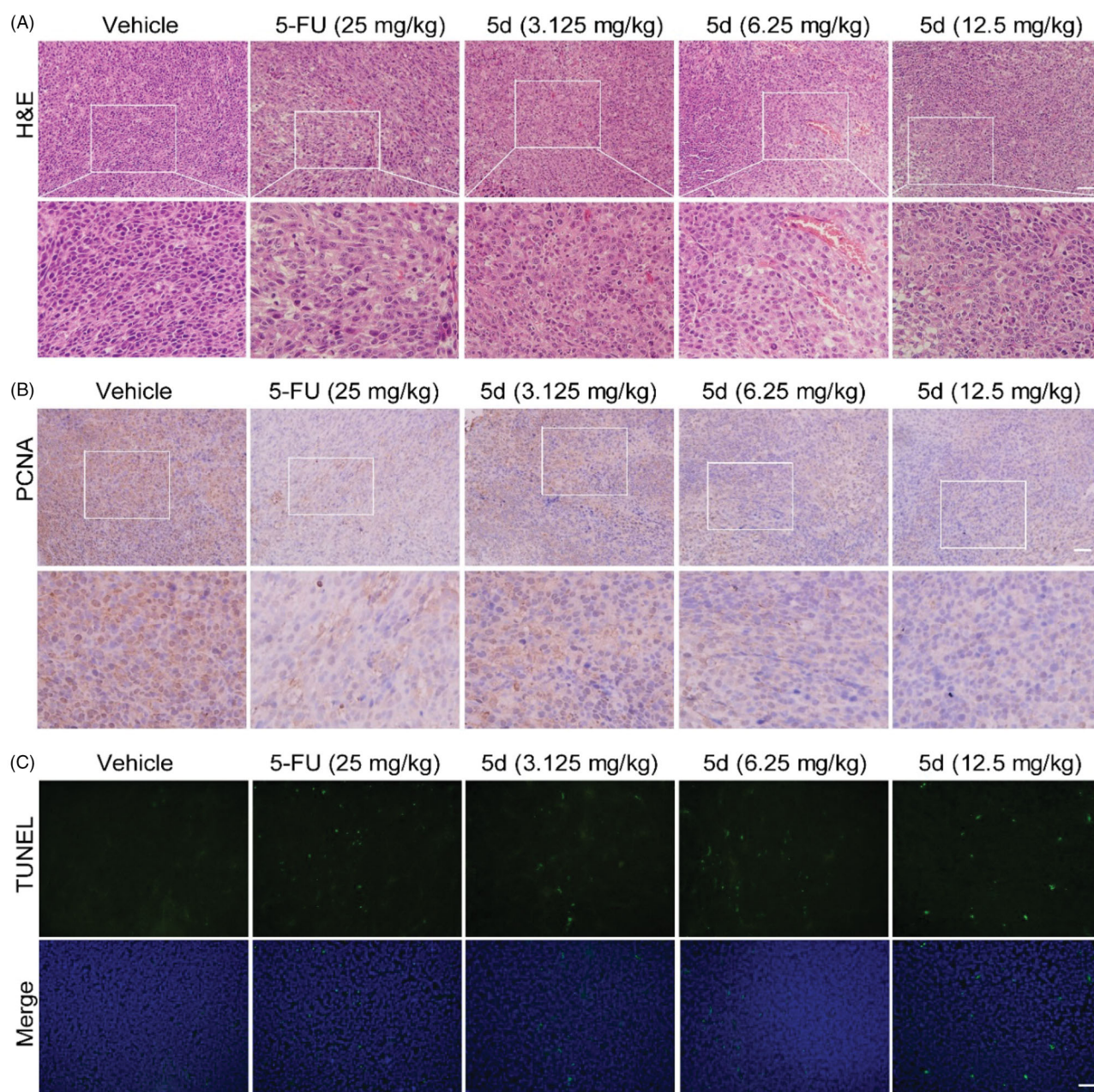


Figure 9. Compound **5d** dose-dependently reduced tumour cells and induced apoptosis in mice. The tumour tissues were infused in formaldehyde solution for paraffin section. (A) H&E staining of tumour tissue. (B) Expression of PCNA. (C) TUNEL staining of tumour sections. Scale bar: 50 μm .

could promote T cell activation, decrease FoxP3⁺ Treg cell population and heighten the function of CTLs.

3.10. Compound **5d** could effectively suppress melanoma growth in immunocompetent mice

In addition, we also utilised a B16F1 melanoma mouse xenograft model to observe the efficacy of compound **5d** on the other tumours. Malignant melanoma is a highly invasive tumour and its immunotherapy has been receiving attention in recent years. As mentioned above, B16F1 is a murine melanoma cell line that expresses IDO1. The mouse xenograft model was established by subcutaneously implanting B16F1 melanoma cells into BALB/c mice and treated with **5d** (3.125, 6.25, 12.5 mg/kg, i.g, every day) or the positive control Cis-platinum (1 mg/kg, i.p, every other day).

Tumour volumes were measured every two days for 11 days. As shown in Figure 13, treatment with **5d** significantly suppressed the growth of tumour in a dose-dependent manner both in tumour volume and in tumour weight as compared with the vehicle group without significant body weight loss. Especially at high dose, the average volume of tumour was reduced by 34.3% after **5d** treatment, which were comparable to Cis-platinum.

Analogously, we also performed H&E, IHC and TUNEL experiments on the B16F1 melanoma tissues (Figure 14 and 15). These results indicated that compound **5d** could effectively contribute to the morphological changes of B16F1 melanoma cells, reduce the number of tumour cells by inhibiting proliferation and inducing apoptosis, and facilitate tumour vascular normalisation. Importantly, compound **5d** also promoted T cell activation by up-regulating IFN- γ expression, and elevated CTLs function by stimulating granzyme B secretion. These results reaffirm that compound

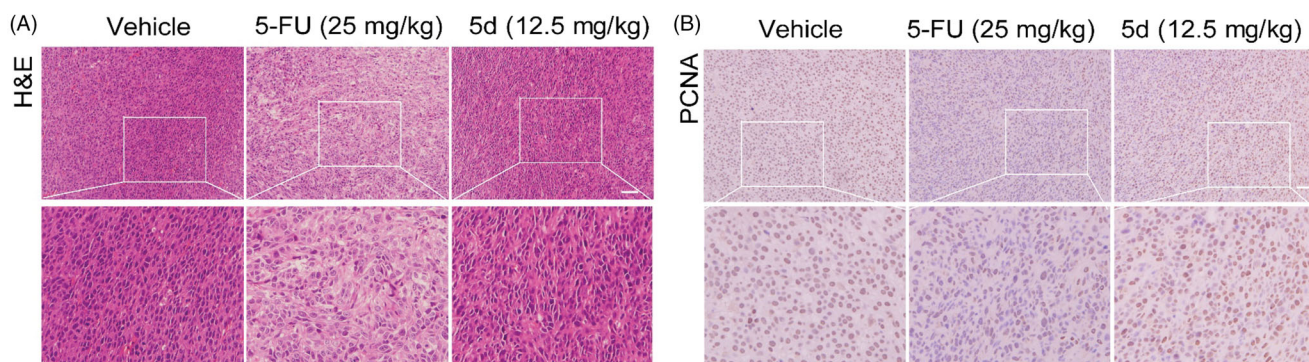


Figure 10. Compound **5d** could not suppress the proliferation of tumour cells in immunodeficient mice. Tumour sections were infused in formaldehyde solution for immunohistochemistry. (A) H&E staining of tumour tissue. (B) Expression of PCNA. Scale bar: 50 μ m.

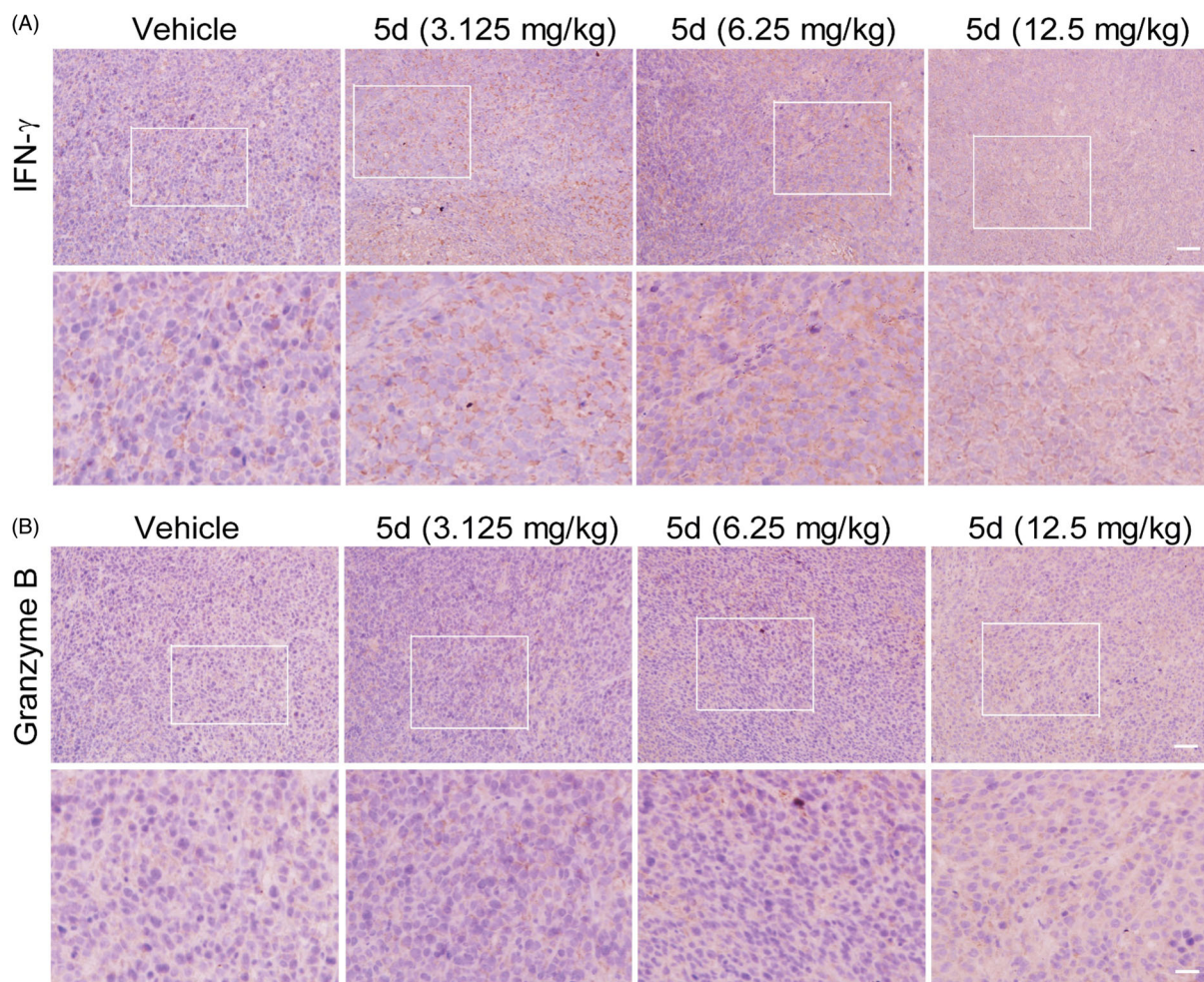


Figure 11. Compound **5d** up-regulated the expression of IFN- γ and granzyme B. Tumour sections were infused in formaldehyde solution for immune stain. (A) Expression of IFN- γ . (B) Expression of Granzyme B. Scale bar: 50 μ m.

5d could inhibit tumour growth by activating the mouse immune system.

3.11. Molecular modelling studies

Based on their outstanding performance in biological activity, we performed computational studies to elucidate the interactions of

compounds **5d** with IDO1. Since the high flexibility of the side chain and backbone of IDO1 protein, the classical semi-flexible docking method often poses a problem for IDO1 docking, whose algorithm relies on a rigid protein structure. Thus, the induced fit docking (IFD) method was utilised to overcome the difficulty mentioned above. The cocrystallization of Amg-1 in complex with human IDO1 protein (PDB ID: 4PK5) was employed as the template in the following docking calculations because of its relatively

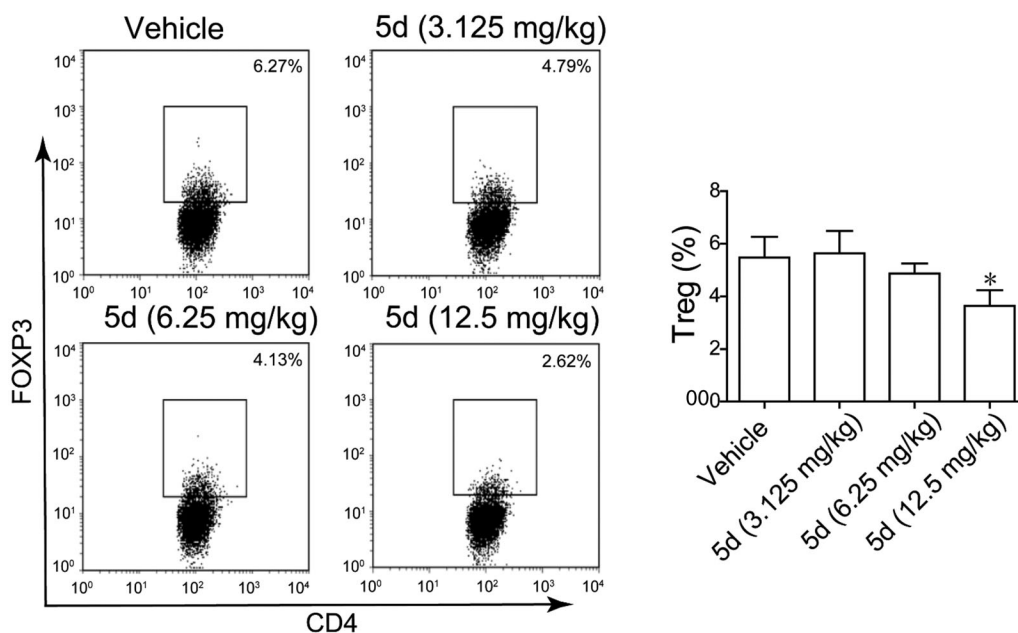


Figure 12. Compound 5d decreased Treg cell differentiation in the CT26 tumour-bearing mouse. (A) Decreased differentiation of Treg cells in the spleen of tumour-bearing mice treated by compounds. (B) Statistical analysis of result A. Data represent mean \pm SEM, * p < 0.05 vs vehicle.

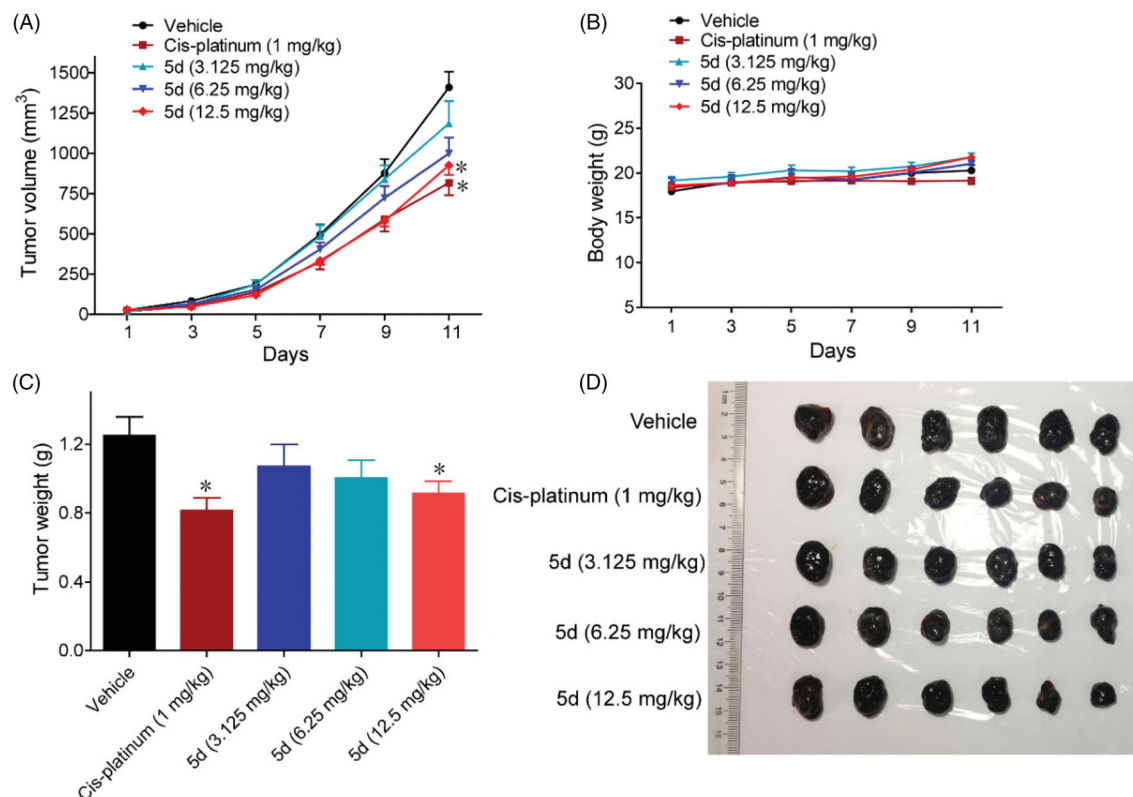


Figure 13. Compound 5d suppressed melanoma growth in mice. 1×10^6 melanoma cells were transplanted subcutaneously into the armpit of the BALB/c mice. Three days after transplantation, mice were randomly allocated to vehicle control or treatment groups ($n = 6$). Drugs were administered on days 1–11. (A) Tumour volume and mouse body weight (B) were recorded. After sacrifice, solid tumours were separated and weighed (C, D). Data represent mean \pm SEM, $n = 6$, * p < 0.05, ** p < 0.01 vs vehicle.

high resolution and more structural information at pocket B. As shown in Figure 16, The benzulfamide moiety situated deeply in pocket A and their benzene ring was interacted with Phe163 through π - π interaction, while the benzylamine moiety extended

towards pocket B formed by Phe163, Phe226, Arg231, Leu234 and Ile354. Specifically, one oxygen atom of the sulphonyl group bond directly to the haem iron of IDO1 while the other oxygen atom formed a hydrogen bond with the main chain NH group of

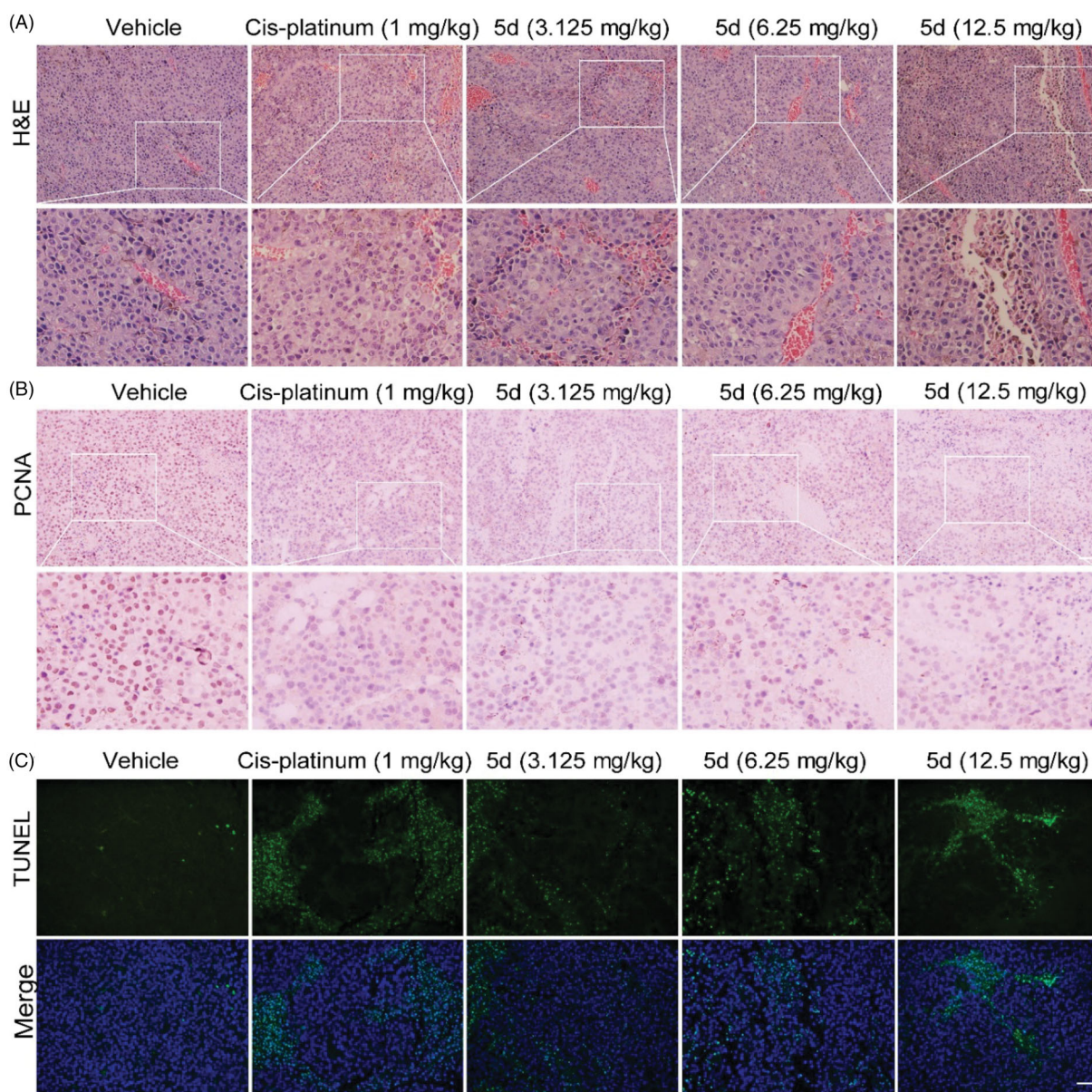


Figure 14. Compound **5d** dose-dependently reduced tumour cells and induced apoptosis in mice. Tumour sections were infused in formaldehyde solution for immunohistochemistry. (A) H&E staining of tumour tissue. (B) Expression of PCNA. (C) TUNEL staining of tumour sections. Scale bar: 50 μ m.

Ala264. Acryloyl groups located at the top of pocket A, and ethenyl moiety of acryloyl group extended towards a small hydrophobic subpocket formed by Met88, Leu124, Cys129, Leu234 and Gly262. This computational study finds that the occupation of the small hydrophobic subpocket in pocket A may be a key factor affecting IDO1 inhibitory activity. These data could be useful for further optimisation.

4. Conclusions

In this study, the hit compound BS-1 was found as an IDO1 inhibitor in-house compound library. After structural optimisation, a series of sulphonamide derivatives were designed, synthesised, and evaluated in the HeLa cell-based IDO1/kynurenine assay, resulting in the identification of secondary sulphonamides as novel IDO1 inhibitors. Among them, the compounds **5d**, **5l** and **8g** displayed

the strongest inhibitory effect, and their activities were significantly improved over the hit compound BS-1. The *in vitro* results showed that these compounds could bind to IDO1 protein in HeLa cells without affecting the cell viability and the IDO1 protein expression under experimental conditions, indicating that these compounds blocked the kynurenine pathway by influencing IDO1 enzyme activity rather than IDO1 expression and/or cell viability. In addition, these compounds could promote the T cell proliferation and suppress the differentiation of naïve CD4⁺ T cell into FoxP3⁺ Treg cells, suggesting that these sulphonamides could reverse IDO1-mediated immunosuppression.

Based on its excellent performance *in vitro*, compound **5d** was selected for further evaluating the pharmacodynamic effects in three types of tumour-bearing mouse models, including two immunocompetent mouse xenografts and one immunodeficient mouse xenograft. These *in vivo* experiments demonstrated that treatment with **5d** could effectively inhibit the growth of murine

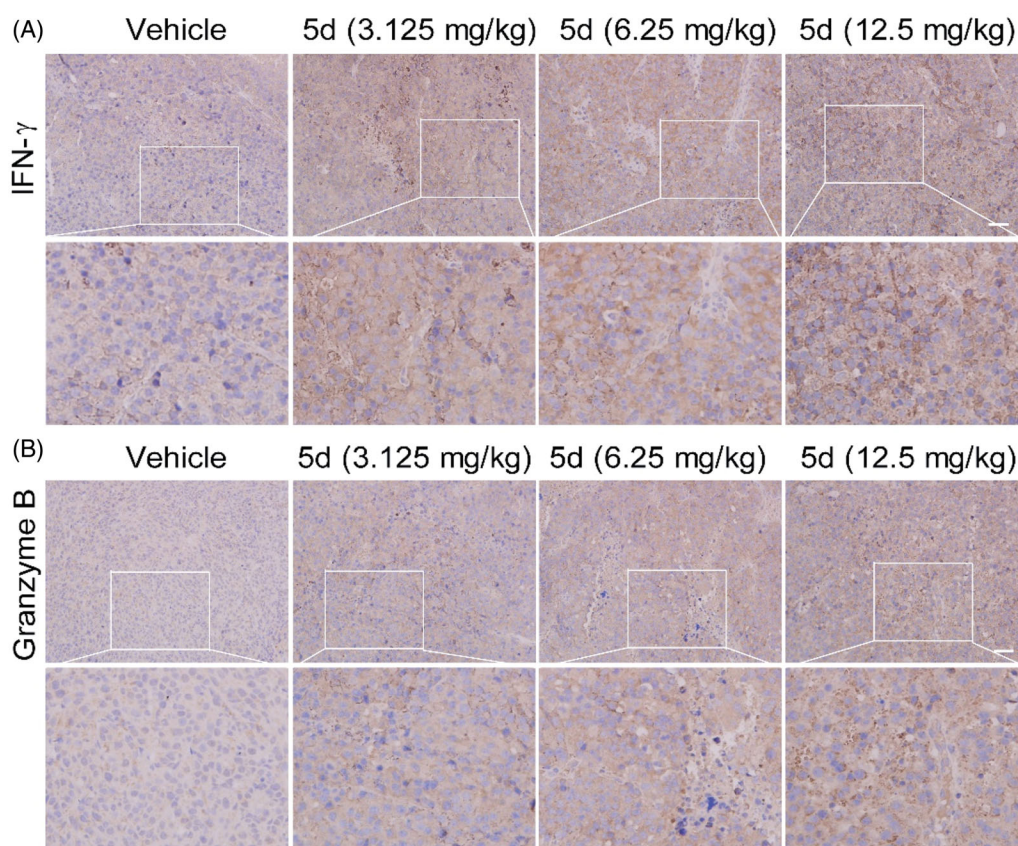


Figure 15. Compound **5d** promoted T cells activation while reduced Foxp3⁺ Treg cell number in tumour tissue. Tumour sections were infused in formaldehyde solution for immune stain. (A) Expression of IFN- γ . (B) Expression of Granzyme B. Scale bar: 50 μ m.

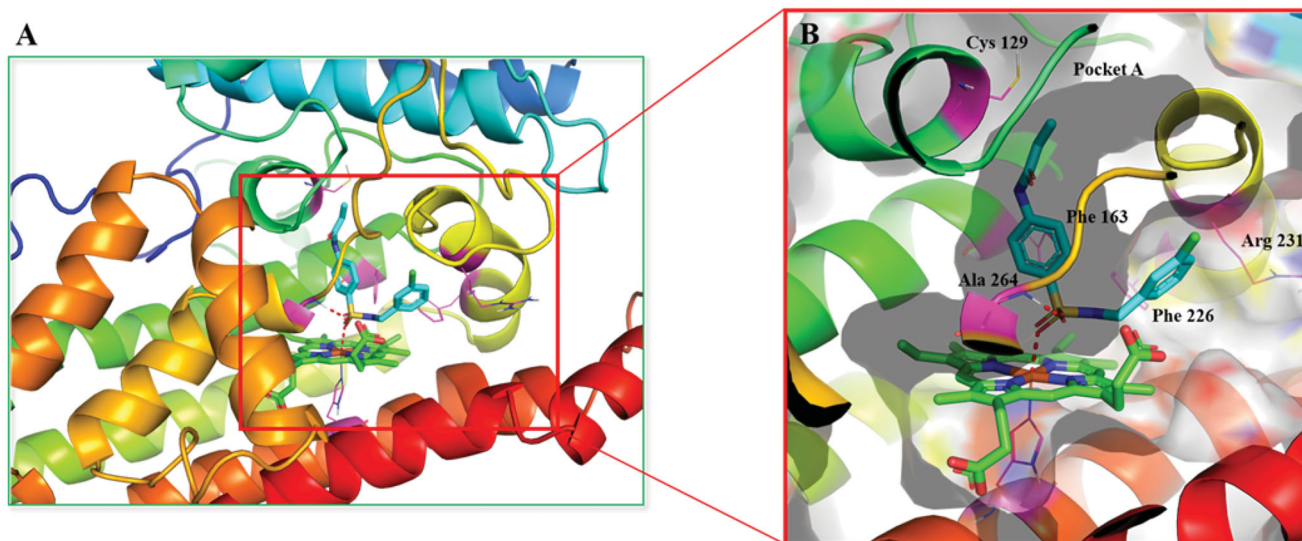


Figure 16. (A) Proposed binding mode of compound **5d** docked into the crystal structure of human IDO1 (PDB: 4PK5) by IFD methods. (B) The interactions between compound **5d** and IDO1. Polar interactions were presented by red dotted line.

CT26 coloreatic carcinoma xenograft tumour in a dose-dependent manner in immunocompetent mice, but not in immunodeficient mice, which implied that the *in vivo* efficacy of compound **5d** was closely associated with the mouse immune system. Similarly, **5d** also significantly blocked the growth of B16F1 melanoma in immunocompetent mice. Functionally, biochemical experiment

and pathological analysis were utilised to detect these tumour tissues. The results from two immunocompetent mouse models indicated that compound **5d** could induce the morphological changes of both CT26 and B16F1 tumour cells, decrease the number of tumour cells by suppressing proliferation and inducing apoptosis. Importantly, compound **5d** could contribute to T cell

activation by stimulating IFN- γ expression, improve CTLs function by inducing granzyme B secretion, and inhibit FoxP3⁺ Treg cell differentiation, which would help facilitate the rejuvenation of the immune system. These promising results motivate us to further develop this new type of IDO1 inhibitors.

Disclosure statement

No potential conflict of interest was reported by the author(s).

Funding

This work was supported by grants from the National Natural Science Foundation of China [No. 21772233, 21977117, 81730100, 21807104 and 81922067], the Natural Science Foundation of Jiangsu Province [No. BK20190306], the Fundamental Research Funds for the Central Universities [No. 2632020TD037 and 2181900125], and the Postgraduate Research & Practice Innovation Programme of Jiangsu Province [No. KYCX18_0790].

ORCID

Shushan Ge  <http://orcid.org/0000-0003-2812-1376>

Wenjie Guo  <http://orcid.org/0000-0001-8506-3905>

Yisheng Lai  <http://orcid.org/0000-0002-8026-7949>

References

- Lizée G, Overwijk WW, Radvanyi L, et al. Harnessing the power of the immune system to target cancer. *Annu Rev Med* 2013;64:71–90.
- Topalian SL, Drake CG, Pardoll DM. Immune checkpoint blockade: a common denominator approach to cancer therapy. *Cancer Cell* 2015;27:450–61.
- Schadendorf D, Hodi FS, Robert C, et al. Pooled analysis of long-term survival data from phase II and phase III trials of ipilimumab in Unresectable or Metastatic Melanoma. *J Clin Oncol* 2015;33:1889–94.
- Szostak B, Machaj F, Rosik J, et al. CTLA4 antagonists in phase I and phase II clinical trials, current status and future perspectives for cancer therapy. *Expert Opin Investig Drugs* 2019;28:149–59.
- Alsaab HO, Sau S, Alzhrani R, et al. PD-1 and PD-L1 checkpoint signaling inhibition for cancer immunotherapy: mechanism, combinations, and clinical outcome. *Front Pharmacol* 2017;8:561.
- Majzner RG, Mackall CL. Clinical lessons learned from the first leg of the CAR T cell journey. *Nat Med* 2019;25:1341–55.
- Kremer KM. Immune checkpoint blockade: a new paradigm in treating advanced cancer. *J Adv Pract Oncol* 2014;5:418–31.
- Cervenka I, Agudelo LZ, Ruas JL. Kynurenines: tryptophan's metabolites in exercise, inflammation, and mental health. *Science* 2017;357:eaaf9794.
- Munn DH, Mellor AL. Indoleamine 2,3 dioxygenase and metabolic control of immune responses. *Trends Immunol* 2013;34:137–43.
- Mándi Y, Vécsei L. The kynurenine system and immunoregulation. *J Neural Transm (Vienna)* 2012;119:197–209.
- Munn DH, Sharma MD, Baban B, et al. GCN2 kinase in T cells mediates proliferative arrest and anergy induction in response to indoleamine 2,3-dioxygenase. *Immunity* 2005;22:633–42.
- Frumento G, Rotondo R, Tonetti M, et al. Tryptophan-derived catabolites are responsible for inhibition of T and natural killer cell proliferation induced by indoleamine 2,3-dioxygenase. *J Exp Med* 2002;196:459–68.
- Mezrich JD, Fechner JH, Zhang X, et al. An interaction between kynurenine and the aryl hydrocarbon receptor can generate regulatory T cells. *J Immunol* 2010;185:3190–8.
- Okamoto A, Nikaido T, Ochiai K, et al. Indoleamine 2,3-dioxygenase serves as a marker of poor prognosis in gene expression profiles of serous ovarian cancer cells. *Clin Cancer Res* 2005;11:6030–9.
- Ino K, Yoshida N, Kajiyama H, et al. Indoleamine 2,3-dioxygenase is a novel prognostic indicator for endometrial cancer. *Br J Cancer* 2006;95:1555–61.
- Pan K, Wang H, Chen MS, et al. Expression and prognosis role of indoleamine 2,3-dioxygenase in hepatocellular carcinoma. *J Cancer Res Clin Oncol* 2008;134:1247–53.
- Folgiero V, Goffredo BM, Filippini P, et al. Indoleamine 2,3-dioxygenase 1 (IDO1) activity in leukemia blasts correlates with poor outcome in childhood acute myeloid leukemia. *Oncotarget* 2014;5:2052–64.
- Speeckaert R, Vermaelen K, van Geel N, et al. Indoleamine 2,3-dioxygenase, a new prognostic marker in sentinel lymph nodes of melanoma patients. *Eur J Cancer* 2012;48:2004–11.
- Liu X, Shin N, Koblisch HK, et al. Selective inhibition of IDO1 effectively regulates mediators of antitumor immunity. *Blood* 2010;115:3520–30.
- Holmgaard RB, Zamarin D, Munn DH, et al. Indoleamine 2,3-dioxygenase is a critical resistance mechanism in antitumor T cell immunotherapy targeting CTLA-4. *J Exp Med* 2013;210:1389–402.
- Tu W, Yang F, Xu G, et al. Discovery of imidazoisoindole derivatives as highly potent and orally active indoleamine-2,3-dioxygenase inhibitors. *ACS Med Chem Lett* 2019;10:949–53.
- Gomes B, Driessens G, Bartlett D, et al. Characterization of the selective indoleamine 2,3-dioxygenase-1 (IDO1) catalytic inhibitor EOS200271/PF-06840003 supports IDO1 as a critical resistance mechanism to PD-(L)1 blockade therapy. *Mol Cancer Ther* 2018;17:2530–42.
- Yue EW, Douty B, Wayland B, et al. Discovery of potent competitive inhibitors of indoleamine 2,3-dioxygenase with *in vivo* pharmacodynamic activity and efficacy in a mouse melanoma model. *J Med Chem* 2009;52:7364–7.
- Markwalder JA, Seitz SP, Blat Y, et al. Identification and optimization of a novel series of indoleamine 2,3-dioxygenase inhibitors. *Bioorg Med Chem Lett* 2017;27:582–5.
- Yue EW, Sparks R, Polam P, et al. INCB24360 (Epcadostat), a highly potent and selective indoleamine-2,3-dioxygenase 1 (IDO1) inhibitor for immuno-oncology. *ACS Med Chem Lett* 2017;8:486–91.
- Williams DK, Markwalder JA, Balog AJ, et al. Development of a series of novel o-phenylenediamine-based indoleamine 2,3-dioxygenase 1 (IDO1) inhibitors. *Bioorg Med Chem Lett* 2018;28:732–6.
- Kumar S, Waldo JP, Jaipuri FA, et al. Discovery of clinical candidate (1R,4r)-4-((R)-2-((S)-6-fluoro-5H-imidazo[5,1-a]isoindol-5-yl)-1-hydroxyethyl)cyclohexan-1-ol (Navoximod), a

- potent and selective inhibitor of indoleamine 2,3-dioxygenase 1. *J Med Chem* 2019;62:6705–33.
28. Brastianos HC, Vottero E, Patrick BO, et al. Exiguamine A, an indoleamine-2,3-dioxygenase (IDO) inhibitor isolated from the marine sponge *Neopetrosia exigua*. *J Am Chem Soc* 2006;128:16046–7.
 29. Yang S, Li X, Hu F, et al. Discovery of tryptanthrin derivatives as potent inhibitors of indoleamine 2,3-dioxygenase with therapeutic activity in Lewis lung cancer (LLC) tumor-bearing mice. *J Med Chem* 2013;56:8321–31.
 30. Platten M, Nollen EAA, Röhrig UF, et al. Tryptophan metabolism as a common therapeutic target in cancer, neurodegeneration and beyond. *Nat Rev Drug Discov* 2019;18:379–401.
 31. Zou Y, Wang F, Wang Y, et al. Systematic study of imidazoles inhibiting IDO1 via the integration of molecular mechanics and quantum mechanics calculations. *Eur J Med Chem* 2017;131:152–70.
 32. Zou Y, Wang Y, Wang F, et al. Discovery of potent IDO1 inhibitors derived from tryptophan using scaffold-hopping and structure-based design approaches. *Eur J Med Chem* 2017;138:199–211.
 33. Zou Y, Wang F, Wang Y, et al. Discovery of imidazoleisindole derivatives as potent IDO1 inhibitors: design, synthesis, biological evaluation and computational studies. *Eur J Med Chem* 2017;140:293–304.
 34. Zou Y, Hu Y, Ge S, et al. Effective virtual screening strategy toward heme-containing proteins: identification of novel IDO1 inhibitors. *Eur J Med Chem* 2019;184:111750
 35. Gaspari P, Banerjee T, Malachowski WP, et al. Structure-activity study of brassinin derivatives as indoleamine 2,3-dioxygenase inhibitors. *J Med Chem* 2006;49:684–92.
 36. Gulçin T, Taslimi P. Sulfonamide inhibitors: a patent review 2013-present. *Expert Opin Ther Pat* 2018;28:541–9.
 37. Penning TD, Talley JJ, Bertenshaw SR, et al. Synthesis and biological evaluation of the 1,5-diarylpyrazole class of cyclooxygenase-2 inhibitors: identification of 4-[5-(4-methylphenyl)-3-(trifluoromethyl)-1H-pyrazol-1-yl]benzenesulfonamide (SC-58635, Celecoxib). *J Med Chem* 1997;40:1347–65.
 38. Cheng MF, Hung MS, Song JS, et al. Discovery and structure-activity relationships of phenyl benzenesulfonylhydrazides as novel indoleamine 2,3-dioxygenase inhibitors. *Bioorg Med Chem Lett* 2014;24:3403–6.
 39. Wang X, Ahn YM, Lentscher AG, et al. Design, synthesis, and evaluation of substituted nicotinamide adenine dinucleotide (NAD⁺) synthetase inhibitors as potential antitubercular agents. *Bioorg Med Chem Lett* 2017;27:4426–30.
 40. Uyttenhove C, Pilotte L, Théate I, et al. Evidence for a tumoral immune resistance mechanism based on tryptophan degradation by indoleamine 2,3-dioxygenase. *Nat Med* 2003;9:1269–74.
 41. Negmeldin AT, Knoff JR, Pflum M. The structural requirements of histone deacetylase inhibitors: C4-modified SAHA analogs display dual HDAC6/HDAC8 selectivity. *Eur J Med Chem* 2018;143:1790–806.
 42. Lin SY, Yeh TK, Kuo CC, et al. Phenyl benzenesulfonylhydrazides exhibit selective indoleamine 2,3-dioxygenase inhibition with potent *in vivo* pharmacodynamic activity and Antitumor Efficacy. *J Med Chem* 2016;59:419–30.
 43. Jin S, Wang F, Zou Y, et al. Design, synthesis and biological evaluation of phenylsulfonamide-based IDO1 inhibitors. *J China Pharm Univ* 2018;49:34–8.
 44. Afonina IS, Cullen SP, Martin SJ. Cytotoxic and non-cytotoxic roles of the CTL/NK protease granzyme B. *Immunol Rev* 2010;235:105–16.
 45. Togashi Y, Shitara K, Nishikawa H. Regulatory T cells in cancer immunosuppression – implications for anticancer therapy. *Nat Rev Clin Oncol* 2019;16:356–71.
 46. Jafari R, Almqvist H, Axelsson H, et al. The cellular thermal shift assay for evaluating drug target interactions in cells. *Nat Protoc* 2014;9:2100–22.
 47. Xu Q, Gu J, Lv Y, et al. Angiogenesis for tumour vascular normalization of Endostar on hepatoma 22 tumour-bearing mice is involved in the immune response. *Oncol Lett* 2018;15:3437–46.
 48. Munn DH, Shafizadeh E, Attwood JT, et al. Inhibition of T cell proliferation by macrophage tryptophan catabolism. *J Exp Med* 1999;189:1363–72.